The Thesis Committee for Wenbin Ouyang
Certifies that this is the approved version of the following thesis:

Evaluating Cotton Maturity Using Fiber Cross-sectional Images

APPROVED BY
SUPERVISING COMMITTEE:

Supervisor:

Bugao Xu

Jonathan Y. Chen

Evaluating Cotton Maturity Using Fiber Cross-sectional Images

by

Wenbin Ouyang, B.E.; M.E.; M.S.T.A.T

Thesis

Presented to the Faculty of the Graduate School of

The University of Texas at Austin

in Partial Fulfillment

of the Requirements

for the Degree of

Master of Science in Engineering

The University of Texas at Austin

August 2016

Abstract

Evaluating Cotton Maturity Using Fiber Cross-sectional Images

Wenbin Ouyang, M.S.E.

The University of Texas at Austin, 2016

Supervisor: Bugao Xu

The cross-section of a cotton fiber provides a directly fiber geometric description. It is known that analysis on a cross-section image will offer a true measure of fiber wall thickness, and derive an accurate cotton fiber maturity evaluation. The fiber image analysis system (FIAS) has been developed for several years. The previous two versions of FIAS were equipped with a traditional microscope with a limited field of view. And the old algorithms were lack of the ability to detect immature fibers correctly, which yielded a systematic bias in the maturity distribution.

In this study, images are captured under a new hardware setup with a wide-field of view and a high-resolution camera. A novel descriptor, coupled-contour model (*CCM*), is introduced to illustrate the relationship between the inner and outer contours of a cotton fiber cross-section. After the detection of the inner and outer contours, triangle-area representation (*TAR*) is used to describe the shape of the cross-section, and to determine whether the cross-section needs further processing. For those cross-sections analyzed

with adhering, self-rolling, scratched, and contaminated characteristics, a cross-section case by case study is required. By analyzed the algorithm efficiency of the randomly picked 7 cottons in 104, it was found the case by case study did occupy about 30% of the whole processing period.

This study investigated all the 104 cottons with 15473 fiber cross-sectional images. By introduced more statistic parameters, including mean (M_θ), standard deviation (SD_θ), skewness (S_θ), and kurtosis (K_θ), a more comprehensive cotton fiber maturity understanding was achieved. According to the maturity distribution, the 104 cottons are distinguishable and divided into 5 classes, i.e. very low, low, moderate, high, and very high from class I to class V, respectively. The comparison made between AFIS and the current FIAS informs that the maturity distributions of AFIS and FIAS are noticeably different. AFIS tends to generate more normal, less skewed and more concentrated maturity distributions but FIAS provides diversified maturity distributions.

.

Table of Contents

List of Tables

List of Figures

Chapter 1: Introduction

1.1 Motivation and Goals

Cotton fiber maturity represented by θ (0-1), the ratio of the cell wall thickness to the overall diameter of the fiber, is one of the most important cotton fiber quality indication. Immaturity and dead fiber will cause in the low dye undertake, weaken yarn strength, fabric defects, and excessive damage and waste during processing [1-3]. Research for calibrating fiber maturity has being done for several decades. Figure 1.1 illustrates the cross-sectional view of a maturity ($\theta \geq 0.6$), an immaturity ($0.3 \leq \theta < 0.6$), and a dead ($\theta < 0.3$) cotton fiber.

(a) Mature (b) Immature (c) Dead

Figure 1.1 Cross-sectional view of different types cotton fibers.

Micronaire (MIC) [4], Advanced Fiber Information System (AFIS) [5], and image analysis on fiber cross-sectional sample are the three major methods for cotton maturity measurement [6-13]. Fiber cross-sectional analysis provides fundamental measurements that are directly related to cotton maturity, and this is the most reasonable approach for developing the cotton-reference database [14]. Fiber Image Analysis System (FIAS) [13] developed by Xu's group helped to expedite the analysis on a large quantity of fiber cross-section images and improved the data reliability for calibrating other testing method. However, a recent independent study revealed that there is an overestimation of the maturity level of bale cotton by around 9% using the laboratory protocol and the

FIAS because 10% to 40% of immature fibers could not be detected correctly in the image processing [15].

Immature fibers, especially dead fibers, have thinner walls, and thus they are more easily scratched or shredded by the cutting blade. They are also likely to be folded up transversely when the lumens collapse, which increases the difficulty of edge detection [16]. After investigating the old FIAS algorithm, we found that the FIAS lacked functions that could automatically separate adhering cross-sections, and misunderstood self-rolling cross-sections as mature fibers. In most cases, adhering cross-sections are eliminated because of their larger size beyond the single cross-section size limitation. Most of the ignored and self-rolling fibers are immature fibers, which cause a systematic bias in fiber detections. When a large number of fibers cannot be detected correctly, the cumulative measurements will not realistically reflect maturity distributions of the sample.

Old FIAS used traditional microscope with a limited field of view. In a modern light microscope, a high-resolution, wide-field digital camera is equipped for fast image acquisition and high-volume fiber property measurements. The old FIAS lacked of the ability to go through all the image pixels captured by the modern light microscope whose view area is approximately 10 times larger than the old microscopic. And the aforementioned problems in cross-sectional detection are intensified in a high-resolution, wide-field image because of its high variability in lighting and focus.

In addition, the mean value of the cross-section data is often used to indicate the maturity level of a sample [13, 14]. In light of the complexity of maturity distributions, the sole-parameter approach does not appear to be reliable and rational for ranking the maturity among different samples.

The principle goal of this study is to design a new cross-section detection algorithm that works for currently high-resolution and wide-field microscope image, and improves the robustness and accuracy of cross sections detection, including the incomplete boundaries and adhering cross-sections, in order to increase the total number of valid measurements and reduce the bias on immature fibers. In the data analysis section, not only the mean value but also the standard deviation and the skewness are taken in to account. A new algorithm to determine the cotton fiber maturity is proposed.

1.2 METHODS FOR COTTON FIBER MATURITY MEASUREMENT

1.2.1 Traditional Evaluation Method

MIC is a measurement of the thickness of the cell walls by calculating the air permeability of a cotton fiber [4]. But both fiber maturity and fineness (weight per unit length) will affect the MIC. Lower MIC cotton could be either immature fibers or fine fibers. A higher MIC may indicate thinner fibers with thick cell walls or coarser fibers [17]. In 1956, Lord setup a relationship between the MIC and the product of fiber linear density and maturity ratio via 100 cotton samples [6, 18], as following,

$$Linear\ Density \times Maturity\ Ratio = 3.86 \times MIC^2 + 18.16 \times MIC + 13 \qquad (1.1)$$

Therefore, without knowing the fineness of fibers, only MIC cannot determinate the fiber maturity.

1.2.2 AFIS Evaluation Method

The AFIS with the help of a high-velocity air flow provide a rapid measurement of single fiber maturity. The fiber maturity and cross-sectional area is analyzed by the light scattered at a 40° angle as fiber flow perpendicularly to the light beam [5]. Although AFIS has a fast measurement processing, its accuracy is questionable compared with the

cross-sectional method. Because twisted mature fibers may fill in the cotton sample, they have large chances to be miscounted as immature fibers by AFIS measurement.

1.2.3 Image Analysis Based Evaluation Method

In 1993, after compared two microscopic methods, cross-sectional and longitudinal scanning of fibers, for characterizing cotton fiber maturity by image analysis, Thibodeaux's group concluded that only the cross-sectional data provided a true measure of a fiber wall thickness [19]. After that, they performed a multi-year project to create a larger-scale cotton-maturity reference by analyzing images of the 104 cotton varieties [14] collected worldwide using a new fiber cross-sectioning protocol [20] and their customized fiber image-analysis system (FIAS) [13].

1.3 COTTON FIBER MATURITY GEOMETRIC MEASUREMENT

Figure 1.2(a) and 1.2(b) show the cross-sectional and the longitudinal view of cotton fibers, respectively. Apparently, cross-sectional image offers a directly measurement of fiber geometry. Four geometric features of a cotton fiber can be directly obtained from figure 1.2(c). The cross-section and lumen perimeters, P_c and P_l, can be obtained by tracing the boundaries on the image. A_c and A_l represent the cross-section and lumen area, which can be calculated by counting all the pixels enclosed inside the two boundaries. The cotton maturity, θ, can be derived from the above measurements [21]:

$$\theta = 4\pi(A_c - A_l)/P_c^2 \tag{1.2}$$

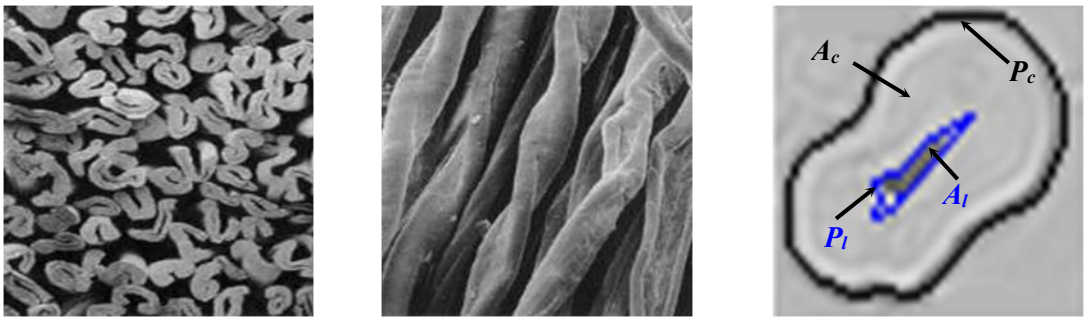

(a) Cross-sectional view (b) longitudinal view (c) Geometry measurements

Figure 1.2 Cotton fiber geometric views.

1.4 STRUCTURE OF THE THESIS

The remainder of the thesis is divided into 5 chapters. Chapter 2 introduces the framework design for the cotton fiber maturity evaluation system. The hardware of microscopic imaging system is presented. The digital camera parameters including resolution, exposure time, and gain are presented. An image example is shown to demonstrate that the current FIAS imaging system has a much wider view area, and a sharper contrast than the previous system.

Chapter 3 points out the previous FIAS system has some potential flaws when detects the adhering, self-rolling, scratched, and contaminated cross-section, and proposes a novel coupled-contour model (*CCM*) for cross-sections analysis. Triangle-Area Representation (*TAR*) is used as a shape descriptor of cross-sections. A case by case study is performed to solve the issues in the old FIAS system.

Chapter 4 exams the cross-section detection accuracy under the proposed algorithm by comparing the results with manual interpretation results. The algorithm efficiency is calculated to evaluate each major step of the algorithm with 7 samples. The error analysis in this chapter is to calculate the error in calculating maturity, and compares the errors of the current detected result with those of the previous study.

Chapter 5 introduces new statistic parameters including standard deviation, skewness, and kurtosis for the 104 cotton samples maturity analysis. System-wise performance is evaluated by comparing with the 104 cottons measurements of AFIS.

Chapter 6 concludes the work and discusses the possible improvements for future study.

Chapter 2: Framework of Cotton Fiber Maturity Evaluation System

The FIAS system is a customized fiber cross-sectional image analysis system for automatic, high volume, and accurate measurements of cotton fiber geometric attributes. A microscope, a digital camera, and a PC consists the whole system. The current FIAS system provides a much larger view area, a deeper contrast, and a more stable light source than the old FIAS imaging system. The microscopic imaging system made using the off-the-shelf hardware is shown in figure 2.1. The Olympus CH30 trinocular phase contrast microscope is used in system for cross-section slides imaging. Besides the binocular eyepiece, this microscope has a vertical eyepiece that is attached to a Canon EOS Rebel T5 digital camera with a camera adapter.

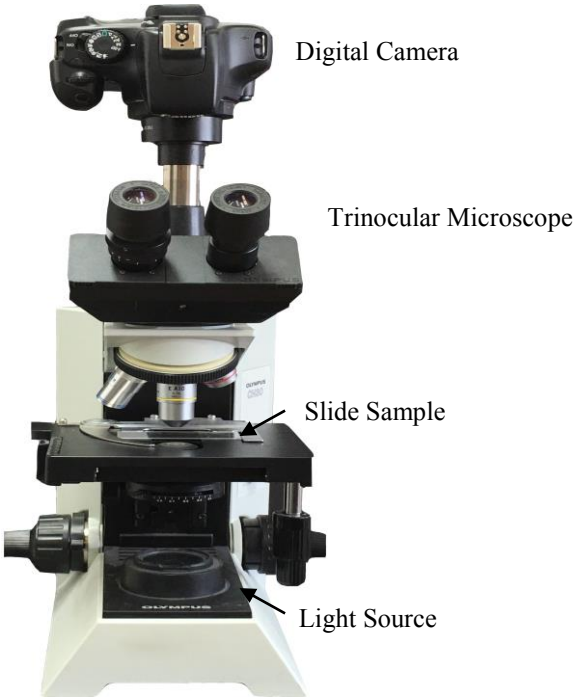

Figure 2.1 Microscope imaging system setup.

The image data is transferred by a USB 2.0 cable connected to a PC. On the PC side, the Canon EOS SDK is used to develop a camera capturing and controlling function for the fiber maturity evaluation software.

An image is captured under 20× objective lens with 2560 × 1920 resolution. A LED light placed underneath the slide provides stable illumination that gives a reliable and consistent intensity of each captured image. The camera exposure time and analog gain are set to a level at which the image background appears to be bright. An example of a captured image is shown in figure 2.2. The microscope view area of the currently system is approximately 10 times larger than the previous system [13, 16].

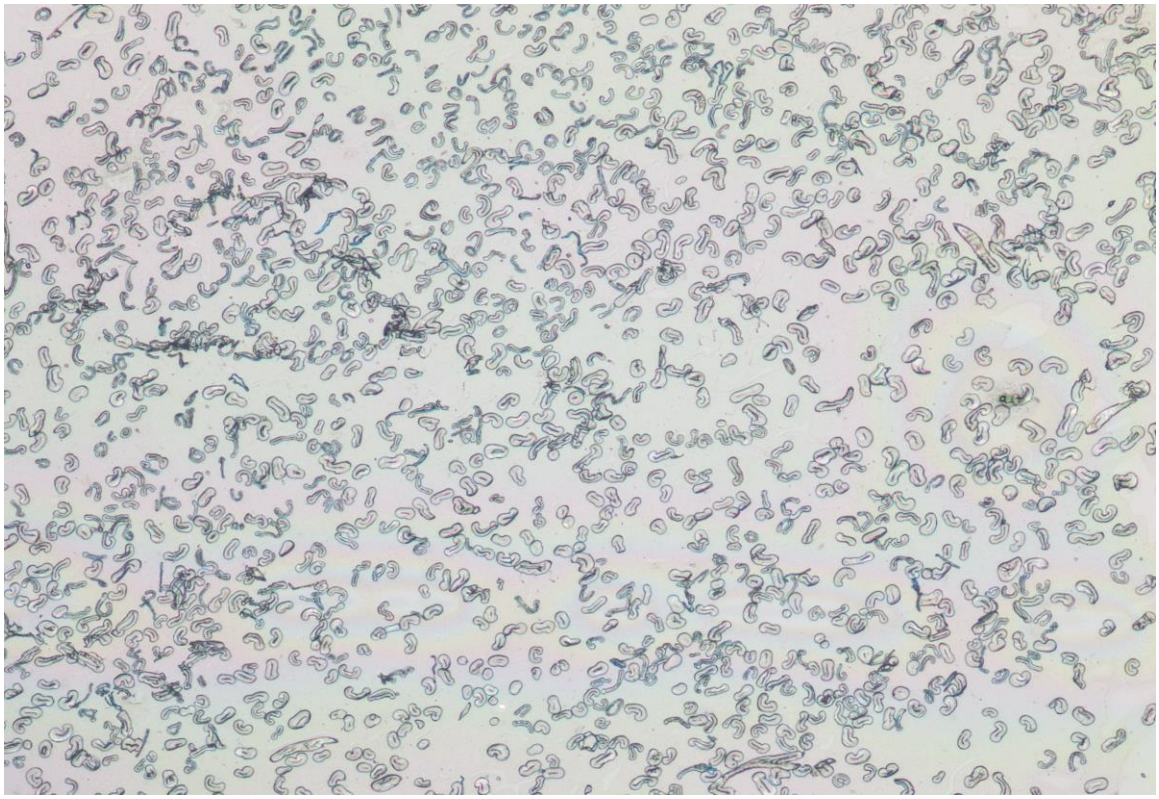

Figure 2.2 An image example captured by the current microscope imaging system.

Chapter 3: Measurement of Cotton Fiber Maturity

3.1 Previous Work

FIAS was developed with 2 generations. FIAS-I [13] proposed four major steps, global dynamic thresholding, background flooding, skeletonzing, and lumen identification , of cotton fiber cross-sectional measurement from a microscope image. The FIAS-I has a reasonable cross-sectional result if there has a uniform image intensity and a higher image contrast. But the detection result is not reliable if the image intensity is bias or a fiber edge is not very sharpness. The second generation FIAS-II [16] did several improvements, including a more reasonable adaptive thresholding method, amending broken edges, and a localized thresholding strategy for lumen identification, which allows the system to detect more fibers and increase the accuracy of the cross-sectional measurement. However, many adhering cross-sections are still neglected due to its larger size, or miscounted as single cross-section for both versions of FIAS. And previous global processing method is no longer suitable for processing a wide-field image containing cross-sections with vastly distinctive shapes and features. A case by case study is needed to improve the cross-section detecting more reliable. Figure 3.1 lists some examples of defective cross-sections and their detected results of FIAS-II, which need further study. Image (a) is a scratched cross-section that had the connected fiber and lumen. Image (b) is a self-rolling cross-section producing wrong cross-sectional perimeter and lumen area, which may result a dead fiber to be counted as a mature fiber. After investigated the 104 cotton fiber image sets, we found that about one out of five cross-sections appeared as self-rolling. Image (c) is a set of adhering cross-sections with a larger area that will be eliminated. Image (d) shows a contaminated cross-section with a

tail that the wrong detected cross-section perimeter caused the abnormal geometric shape of a cotton fiber.

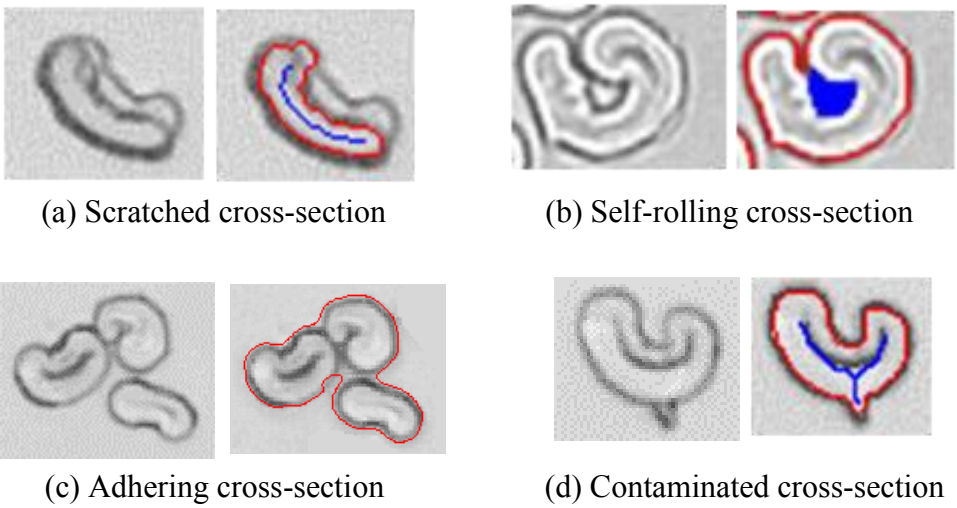

(a) Scratched cross-section (b) Self-rolling cross-section

(c) Adhering cross-section (d) Contaminated cross-section

Figure 3.1 Defective cross-sections and detection results from previous FIAS.

3.2 NEW FIBER CROSS-SECTION GEOMETRIC DESCRIPTOR

Unlike the previous FIAS cross-section model only tracing the cross-section contour and lumen contour, as shown in figure 1.2(c), a new named coupled-contour model (*CCM*) [22] is introduced in figure 3.2. For a typical cotton cross-section, three contours can be generated: fiber outer contour–c_o, fiber inner contour– c_i, and lumen contour–c_l. Of a normal fiber cross-section, c_o and c_i are two concentric parallel contours that should have very similar geometric shape and be very close to each other. Usually, the thickness between c_o and c_i is vary from 2 pixels to 6 pixels depended on the cross-section thickness of prepared samples and the slide focusing status. A new descriptor of a cross-section can be depicted as a triple contour set (c_o, c_i, c_l).

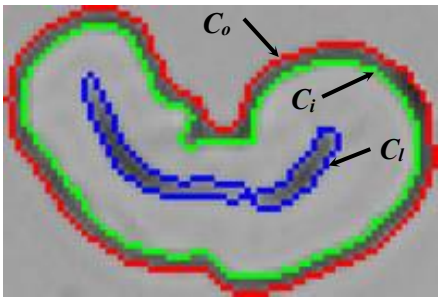

Figure 3.2 Triple contours of a cross-section.

The outer contour detection method is inherited from the previous FIAS adaptive thresholding equation [16]:

$$T_i = M_i - coef_i \times SD_i , \tag{3.1}$$

$$coef_i = 0.014\, M_i - 2.694. \tag{3.2}$$

where T_i is the threshold that is determined by the mean M_i, the location-dependent coefficient $coef_i$, and the standard deviation SD_i of pixel i intensities in the 7×7 sub-window. $coef_i$ is calculated from an empirical equation for based on M_i.

With the roughly detected outer contour c_o, of all the pixels *I(i)* inside the $Region(c_o)$, it is able to calculate an average regional threshold, $T_{Region(c_o)}$, as,

$$T_{Region(c_o)} = \frac{\sum_{I(i)\in Region(c_o)} T_i}{N} \tag{3.3}$$

where N is the number of pixels of $Region(c_o)$. A tolerance ΔT is given when performing the segmentation. The regional threshold range can be represented as $[T_{Region(c_o)} - \Delta T, T_{Region(c_o)} + \Delta T]$. After the segmentation, $C_{2\Delta T}$ is used to depicted all detected contours in c_o. An optimized contour c_o' of c_o is calculated as,

$$c_o' = \underset{\substack{c\in C_{2\Delta T} \\ Region(c)\supset Region(c_o) \\ BBox(c)\cong BBox(c_o)}}{argmin} Length(c), \tag{3.4}$$

where $BBox(c)$ is the function calculating the bounding box of c. $BBox(c) \cong BBox(c_o)$ implies that the difference between the bounding boxes of c and c_o is smaller than a pre-specified value, which is set to 4 pixels in this research. If C_c denotes a set of contours enclosed by c_o, then the set of optimized inner contours $C^i_{c'_o}$ within c'_o can be detected by:

$$C^i_{c'_o} = \left\{ c \middle| \begin{matrix} (c \in C_c \cup C_{2\Delta T}) \wedge (Region(c'_o) \supset Region(c)) \\ \wedge\, (\nexists c' \in C_c \cup C_{\Delta T} (Region(c') \supset Region(c))) \end{matrix} \right\}. \quad (3.5)$$

For any inner contour $c_i \in C^i_{c'_o}$, lumen contours, $C^l_{c'_o}$, can be also found by:

$$C^l_{c'_o} = \{c | (c \in C_c\ ) \wedge (Region(c_i) \supset Region(c))\}. \quad (3.6)$$

Figure 3.3 shows *CCM* based contour detection results of figure 3.1. Apparently, the inner contour c_i provide more useful information, i.e. a further merging or splitting processing need to be performed for image (a), a more accurate contour describing the cross-section shape for image (b) and (d), and adhering cross-sections can be separated in image (c).

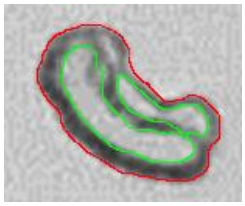

(a) Scratched cross-section

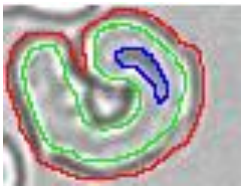

(b) Self-rolling cross-section

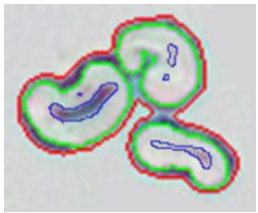

(c) Adhering cross-section

(d) Contaminated cross-section

Figure 3.3 *CCM* detection results on defective cross-sections.

3.3 CONTOURS SHAPE RECOGNITION OF A CROSS-SECTION

To identify and compare c_o and c_i shape is a very important procedure to determine whether the cross-section is normal or it needs further analysis. In this research, a contour， c (e.g., c_o, c_i, or c_l), is an 8-connected closed plane curve.

Triangle-Area Representation (*TAR*) can be harnessed to gain the shape information of a closed plane curve based on three vertices on the curve, and the *TAR* is invariant to translation, rotation, and scaling [23] [24, 25, 26]. Let *P* represent a series of closed boundary points, starting from the most left-low point and in the counterclockwise direction, that is,

$$P = \{p_i(x_i, y_i)\} \tag{3.7}$$

If the total number of boundary points is *N*, step length *t* ($1 \leq t < N/2$) can be used to choose three points $p_i(x_i, y_i)$ to its left and right points $p_{i-t}(x_{i-t}, y_{i-t})$ and $p_{i+t}(x_{i+t}, y_{i+t})$ from series *P*, and the area of the triangle defined by these three vertexes can be calculated as:

$$S_{i,t} = \frac{1}{2} a \times b \times T(\theta_{i,t}) \tag{3.8}$$

where a is the length of $\overline{p_{i-t}p_i}$, b is the length of $\overline{p_i p_{i+t}}$, $\theta_{i,t}$ is the vertex angle between $\overline{p_{i-t}p_i}$ and $\overline{p_i p_{i+t}}$ ($0° \leq \theta_{i,t} \leq 360°$). $S_{i,t}$ is the *TAR* value at point *i* and step length *t*. When *t* varies, multi-scale *TAR* can be expressed as:

$$TAR = \{tar_{i,t}\} \qquad (0 \leq i < N, 1 \leq t < N/2) \tag{3.9}$$

where:

$$tar_{i,t} = S_{i,t}/t \tag{3.10}$$

Using $T(\theta_{i,t})$ instead of $\sin\theta_{i,t}$ in equation 3.8 is because the $\sin\theta_{i,t}$ tendency changing contradicts with the actual change in convexity when $\theta_{i,t} \in (0°, 90°) \cup (270°, 360°)$. In these ranges, the smaller the vertex angle $\theta_{i,t}$, the larger the angle

convexity, which is opposite to the change in *TAR*. In order to form a monotonically declining tendency within the range [0°, 360°], a transformation equation $T(\theta_{i,t})$ can be represented as:

$$T(\theta_{i,t}) = \begin{cases} 2 - \sin\theta_{i,t} & 0° \leq \theta_{i,t} \leq 90° \\ \sin\theta_{i,t} & 0° < \theta_{i,t} \leq 270° \\ -2 - \sin\theta_{i,t} & 270° < \theta_{i,t} \leq 360° \end{cases} \quad (3.11)$$

In $T(\theta_{i,t})$, the original $\sin\theta$ values in (0°, 90°) and (270°, 360°) are modified to be symmetrical to the axes of *y*= 1 and *y*= -1, respectively to guarantee the magnitude value in these two intervals be enhanced dramatically, as seen in figure 3.4.

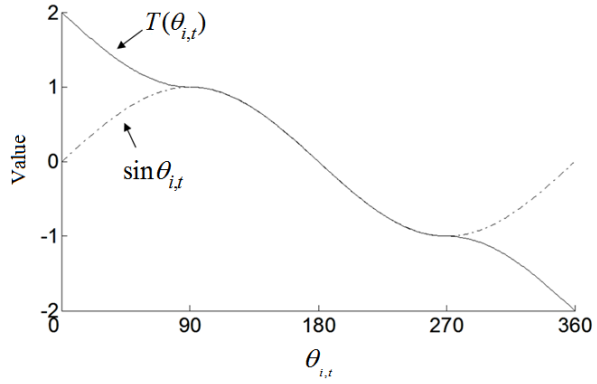

Figure 3.4 $\boldsymbol{T(\theta_{i,t})}$ curvature.

TAR can be positive, negative or zero values, indicating that the three vertices are convex, concave or straight-line points, respectively. The positive values in equation 3.9 can be denoted as $TARP = \{tarp_{i,t}\}$, where

$$tarp_{i,t} = \begin{cases} tar_{i,t}, & tar_{i,t} > 0 \\ 0, & \text{elsewhere} \end{cases} \quad (0 \leq i < N, 1 \leq t < N/2) \quad (3.12)$$

The negative values in equation 3.9 can be marked as $TARN = \{tarn_{i,t}\}$, where

$$tarn_{i,t} = \begin{cases} tar_{i,t}, & tar_{i,t} < 0 \\ 0, & \text{elsewhere} \end{cases} \quad (0 \leq i < N, 1 \leq t < N/2) \quad (3.13)$$

When three vertices are collinear, $TARO = \{taro_{i,t}\}$, where

$$taro_{i,t} = \begin{cases} 0, & tar_{i,t} = 0 \\ 1, & \text{elsewhere} \end{cases} \quad (0 \leq i < N, 1 \leq t < N/2) \quad (3.14)$$

Examples of *tarp*, *tarn* and *taro* points are labeled on a closed shape in figure 3.5(a), and its *TAR* values are drawn in figure 3.5(b) when step length t = 1 in equation 3.10. In figure 3.5(b), the *X* axis represents all the boundary points $0 \leq i < 336$, and the *Y* axis represents the corresponding *TAR* output when t = 1. The *TAR* output clearly shows convexities, concavities and collinear points.

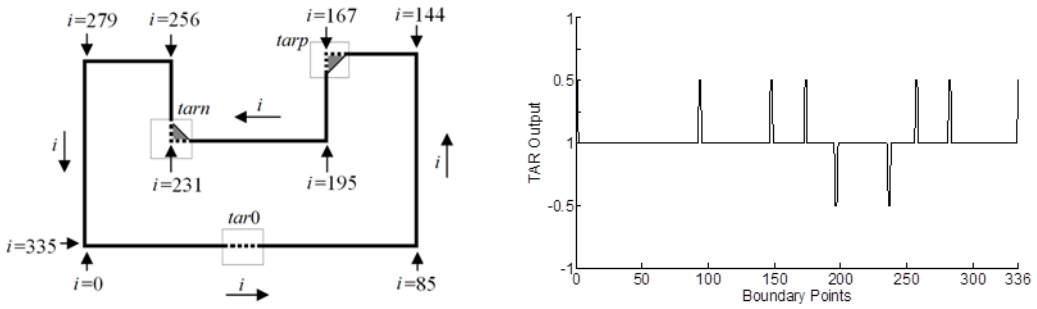

(a) (b)

Figure 3.5 (a) Examples of *tarp*, *tarn*, and *taro* points on a closed boundary. (b) *TAR* output when t=1.

When both boundary point i and step length t vary along a closed boundary, *TARP* and *TARN* outputs can be expressed in grayscale images, as shown in figure 3.6. Figure 3.6(a) and (b) are *TARP* and *TARN* images of the closed boundary in figure 3.5(a) when $0 \leq i < 336$ (the *x*-axis) and $1 \leq i < 168$ (the *y*-axis). Points that have higher absolute *TARP* or *TARN* values are assigned with lower grayscales in the images, and they indicate higher possibility to be convex or concave points in the further process. A white point in the images represents a zero *TARP* or *TARN* value at the current i and t.

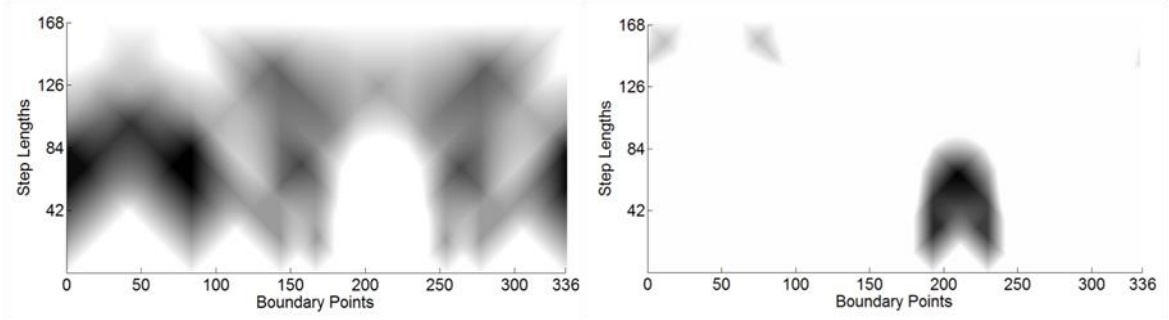

(a) (b)

Figure 3.6 (a) *TARP* and (b) *TARN* image of the closed boundary in figure 3.5.

On a closed boundary, only those protruding or depressing points whose inflection magnitudes exceed certain thresholds can be chosen as convexities or concavities. The protruding magnitude or the depressing magnitude of a boundary point can be measured using its *TARP* or *TARN* values. We will use an average-filter to suppress noise points with small *TARP* or *TARN* values.

When the step length is *t*, and there are *K* ($K \geq 0$) points of positive values in *TARP* output, the average protruding value is:

$$A_t = \frac{1}{K}\sum_i tarp_{i,t} \quad (0 \leq i < N) \tag{3.15}$$

The difference of the *TARP* value at one boundary point from the average protruding value is denoted as $\Delta A_{i,t}$. When $\Delta A_{i,t}$ is above zero, the point is on a convex curve. Thus, we can define the following parameter to describe the convexity of the boundary:

$$AVG-TARP = \begin{cases} \Delta A_{i,t} = tarp_{i,t} - A_t \ , \ \Delta A_{i,t} > 0 \\ 0, \qquad\qquad\qquad \text{elsewhere} \end{cases} \tag{3.16}$$

Similarly, the average depressing value can be represented as:

$$B_t = \frac{1}{K}\sum_i tarn_{i,t} \quad (0 \leq i < N) \tag{3.17}$$

At the same step length, the difference between *TARN* value and its average depressing result is *AVG-TARN*, which is defined as follows:

$$AVG-TARN=\begin{cases}\Delta B_{i,t}=tarn_{i,t}-B_t\ , & \Delta B_{i,t}<0\\ 0, & \text{elsewhere}\end{cases} \tag{3.18}$$

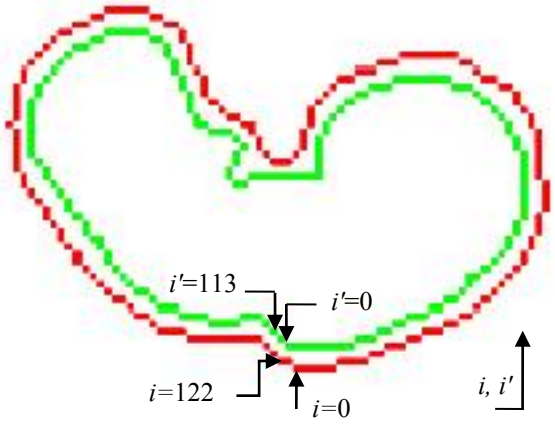

(a) *TAR* calculating direction

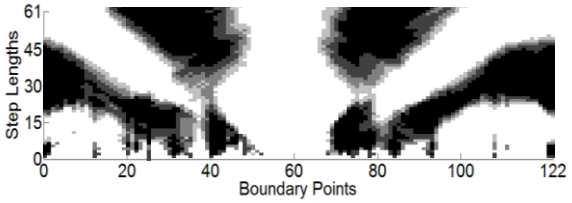

(b) *AVG-TARP* image of c_o

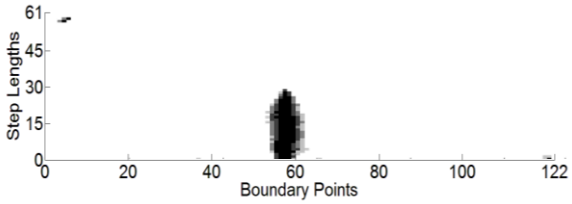

(c) *AVG-TARN* image of c_o

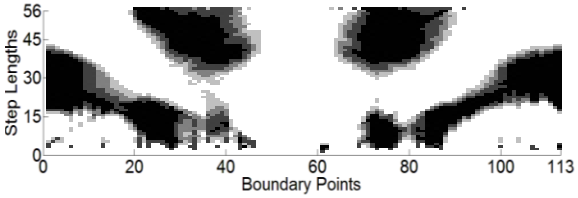

(d) *AVG-TARP* image of c_i

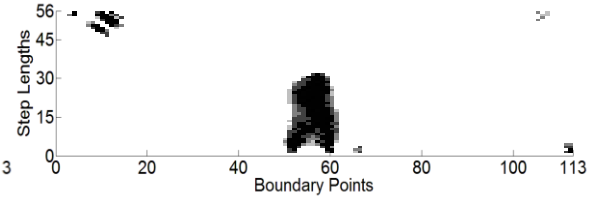

(e) *AVG-TARN* image (e) of c_i

Figure 3.7 *AVG-TARP* and *AVG-TARN* patterns of the cross-section in figure 3.2.

The *TAR* calculating starts from the most bottom-right point on the contour, and searches points counter-clock wise, illustrated in figure 3.7(a). *AVG-TARP* and *AVG-TARN* outputs of the outer contours can be presented in grayscale images when $0 \le i < 122$ in the Boundary-axis and $0 \le t < 61$ in the *Step Lengths*-axis in figure 3.7(b) and (c). The similar images of *AVG-TARP* and *AVG-TARN* inner contours outputs with $0 \le$

$i' < 113$ and $0 \leq t' < 56$ are shown in figure 3.7(d) and (e). By comparing the inner and outer *TAR* patterns, we can easily determine that the outer and inner contours of the cross-section have similar shapes. However, *AVG-TARP* and *AVG-TARN* images provide disordered and diffused grayscale points that are difficult to be translated into convexity or concavity information. The *AVG-TARP* and *AVG-TARN* values at one boundary point can be accumulated along the step length to provide more explicit convexity or concavity information for recognition. The proposed *TAR* histogram is a way to accumulate weighing coefficients of *AVG-TARP* or *AVG-TARN* values through all step lengths. The contribution of the *i*th boundary point to the convexity or concavity, $Weigh_i$, is regarded as the frequency at point *i* in the histogram, and it is expressed as:

$$Weigh_i = \sum_{i=1}^{N/2} w_{i,t} \tag{3.19}$$

where $w_{i,t}$ represents the weighing coefficient of the *i*th boundary point at the current step *t*. In this project, $w_{i,t}$ was assigned with different values based on the difference between its *AVG-TARP* (or *AVG-TARN*) value and the average protruding value A_t (or the average depressing value B_t):

$$\begin{cases} w_{i,t} = 2.0 & AVG - TARP \geq A_t & or & AVG - TARN \leq B_t \\ w_{i,t} = 1.5 & AVG - TARP \geq 0.6A_t & or & AVG - TARN \leq 0.6B_t \\ w_{i,t} = 1.0 & AVG - TARP \geq 0.3A_t & or & AVG - TARN \leq 0.3B_t \\ w_{i,t} = 0.5 & AVG - TARP > 0 & or & VG - TARN < 0 \end{cases} \tag{3.20}$$

Figure 3.8(a)-(d) show the *TARP* and *TARN* histograms obtained from figure 3.7 (b)-(e), respectively. These histograms contain discontinued clusters along the boundary points, each showing a sub-histogram of a convexity or concavity. The starting and ending points of a sub-histogram on the Boundary-axis indicate the boundary range of each convexity or concavity. Meanwhile, the local maximums on the Frequency-axis signify points that possess the highest convexities or concavities in their vicinities on the

boundary. Each of these points can be denoted as a corner point, i.e., the tip of a convex segment. From *TARP* and *TARN* histograms of the cross-shape fiber in figure 3.7(a), two convex (triangle) and one concave points (circle) on both outer and inner contour can be located, as seen in figure 3.8(e).

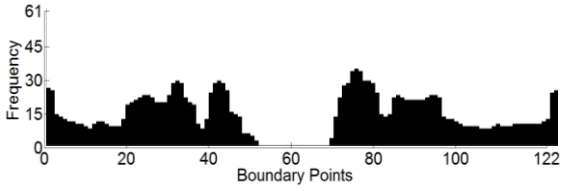

(a) *TARP* histogram of c_o

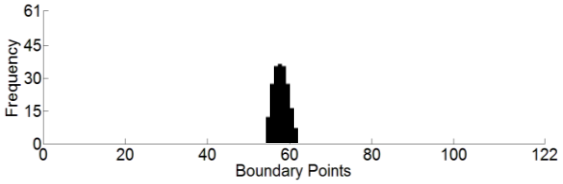

(b) *TARN* histogram of c_o

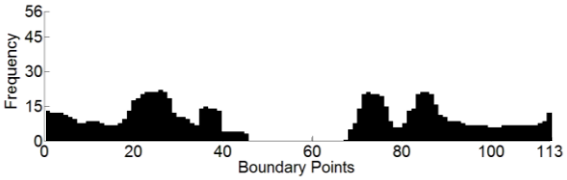

(c) *TARP* histogram of c_i

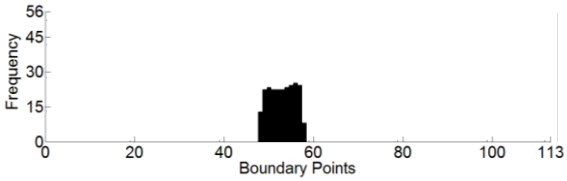

(d) *TARN* histogram of c_i

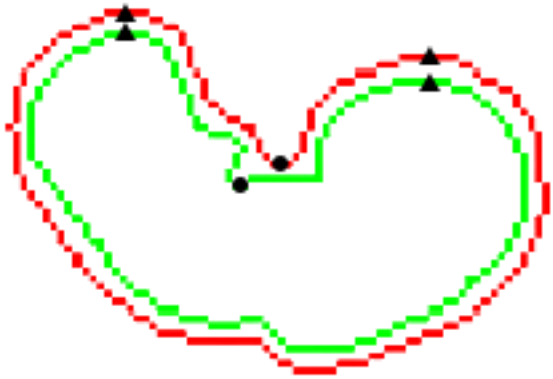

(e) Convex and concave points calculation result

Figure 3.8 Histogram based convexity and concavity recognition of the cross-section in figure 3.2.

The detected concave and convex points of c_o and c_i are denoted as *Concave_*c_o = {(i_1,j_1), (i_2,j_2),... (i_N,j_N)}, *Convex_*c_o = {(i_1,j_1), (i_2,j_2),... (i_N,j_N)}, *Concave_*c_i = {(i_1,j_1), (i_2,j_2),... (i_N,j_N)}, and *Convex_*c_i = {(i_1,j_1), (i_2,j_2),... (i_N,j_N)}, respectively.

3.4 CROSS-SECTION FURTHER PROCESSING METHODS DETERMINATION

With the detection of the c_o and c_i, and the *TAR* analysis result, we are able to determine the further processing case by case. Five criteria, $Q_1(c_o)$, $Q_2(c_i)$, $Q_3(c_o, c_i)$, $Q_4(Convex\_c_o, Convex\_c_i)$, and $Q_5(Concave\_c_o, Concave\_c_i)$ can be expressed as a function, $Q(\cdot)$,

$$\begin{aligned} Q_{1,2}(c) &= \left(T_L^{min} \le Length(c) \le T_L^{max}\right) \\ &\quad \&\&\left(T_A^{min} \le Area(c) \le T_A^{max}\right) \\ &\quad \&\&(Number(C) = 1), \\ Q_3(c_o, c_i) &= \left(Length(c_i) \le Length(c_o)\right), \\ Q_{4,5}(Shape\_c_o, Shape\_c_i) &= \begin{pmatrix} Paired\left(Shape_{C_o}, Shape_{C_i}\right) \\ \ge \ max(N\_c_o, N\_c_i) - 1 \end{pmatrix} \end{aligned} \tag{3.21}$$

where T_L^{min} and T_L^{max} are the upper and lower of contour length thresholds, T_A^{min} and T_A^{max} the upper and lower area thresholds. N_c_o and N_c_i represent the detected concave or convex points on the contours. $Paired(Shape\_c_o, Shape\_c_i)$ is the function of calculating the numbers of concave or convex points that have similar locations in $Shape\_c_o$ and $Shape\_c_i$. The similar location is defined as $|i_o\text{-}i_i| \le 5$ && $|j_o\text{-}j_i| \le 5$ in this research.

Based on the above five criteria results, following processing strategies will be performed:

(a). If Q_1, Q_2, Q_3, Q_4, and Q_5 are all true, no further processing will be required.

(b). If Q_1 and Q_2 are true, but Q_3, Q_4, and Q_5 are false, the inner contour may contain a part of lumen contour, and a splitting process is required.

(c). If only Q_1 is true, this will indicate that more than one inner contours are detected, and a merging process is necessary.

(d). If Q_1, Q_2, and Q_5 are true, but Q_3 and Q_4 are false, the cross-section will be a self-rolling one. The inner contour should be used as the maturity calculation reference.

(e). If Q_1, Q_2, Q_3, and Q_5 are true, only Q_4 is false, the cross-section may be contaminated. A tail cutting on the outer contour is needed.

(f). If Q_1, Q_2, Q_3, Q_4, and Q_5 are all false, this must be the adhering case. Further splitting processes are required.

3.5 CROSS-SECTION CASE BY CASE STUDY

3.5.1 Splitting Inner Contours

As seen in figure 3.9(b), only one inner contour is found, and more concave (triangle indicated) or convex (circle indicated) points of inner contour are detected than the points of outer contour. Only one $Paired(Shape_{C_o}, Shape_{C_i})$ (green dash circle) can be found, which results Q_4(*Convex_c*$_o$, *Convex_c*$_i$), and Q_5(*Concave_c*$_o$, *Concave_c*$_i$) are false. Apparently, the unpaired concave points on the inner contour can be used to form the splitting line. Define $I_{unpaired}$ as the set of the unpaired concave points on the inner contour. After picking all the possible combination of two points (P_i, P_j) in $I_{unpaired}$, a splitting-lines $Line_{split}(P_i, P_j)$ set is generated. For each splitting-line, the inner contour region will be separated into two sub-regions, defined as *Sub_Region*(*smaller*) and *Sub_Region*(*bigger*). If two sub-regions satisfy,

$$Sub\_Region(smaller) \in Sub\_Region(bigger) \tag{3.22}$$

then P_i and P_j can define a valid split, which is denoted as,

$$Split_{c_i}(P_i, P_j) = \{Sub\_Region(smaller), Sub\_Region(bigger)\} \tag{3.23}$$

The $Sub\_Region(bigger)$ is the new inner contour (c_i) and the new lumen contour (c_l) is $Sub\_Region(smaller)$. We double check the *TAR* result on the new inner and outer contours, and find that after performing splitting processing, both inner and outer contours have similar *TAR* pattern and the detected concave/convex points is paired as seen in figure 3.9(c).

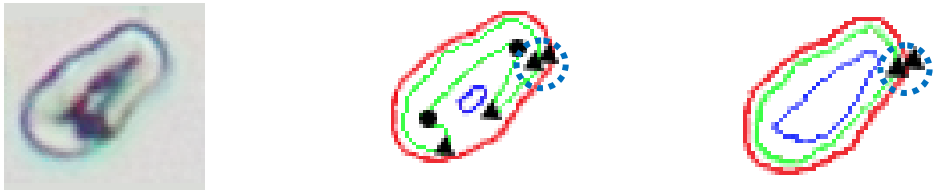

(a) (b) (c)

Figure 3.9 (a) A cross-section with inner contour noise. (b) Detected contours without correction. (c) Corrected inner contour and lumen contour.

3.5.2 Merging Inner Contours

If the outer contour length is within the desired range but more than one inner contours are detected, this case will be considered as broken inner contours, as seen figure 3.3(a). By merging inner contours, a proper lumen contour will be obtained.

The same as the splitting the inner contour case, despite the paired concave points (in the blue dash circle in figure 3.10(a)), the unpaired concave points $I_{unpaired}$ on the inner contour will be used to form merging lines. A merging line set $Line_{merge}(P_i, P_j)$ is formed by all the combination of two points from different inner contours in $I_{unpaired}$. For each merging line, the newly created line pixels is defined as $I_{line\_merge} = \{p_k\}$. Let $C_{c_i} = \{c_i^0, c_i^1, \dots, c_i^N\}$ represent region pixels of the inner contours. A correct merging line should satisfy that the line should not pass through any inner contour area, and can be represented as,

$$I_{line\_merge} \cap C_{c_i} = \emptyset \tag{3.24}$$

From figure 3.3(a), three merging lines is selected (marked with blue lines in figure 3.10(b)), and a merged inner contour and a new lumen contour present in figure 3.10(c).

(a) (b) (c)

Figure 3.10 (a) Cross-section with broken inner contours and more inner concave points. (b) Selected merging lines. (c) Merged inner contour and new formed lumen contour.

3.5.3 Refining Self-rolling and Contaminated Cross-sections

For situations of a self-rolling (figure 3.3(b)) or contaminated cross-section (figure 3.3(d)), we concentrate on comparing the inner and outer contour length and the convex points on both contours. Both situations pass the cross-section size checking, and the outer contour region is slightly bigger than the region inside the inner contour. But by comparing the contours lengths, the self-rolling cross-section presents a longer inner contour length than its outer contour. In order to distinguish the self-rolling from the splitting inner contour case, it is found that the detected concave points on the inner and outer contours are paired, as seen the blue circles in figure 3.11(b). The only unpaired convex points in red box in figure 3.11(b) is because the *y* direction distance is beyond the threshold. It is clear that, for a self-rolling cross-section (figure 3.11(a)), the detected inner contour has a more accurate geometry description. To achieve a more correctly detection result, we manually dilate the inner contour area for 2 pixels. The refining result

of the cross-section is shown in figure 3.11(c). The lumen refinement processing will be discussed in chapter 3.6.

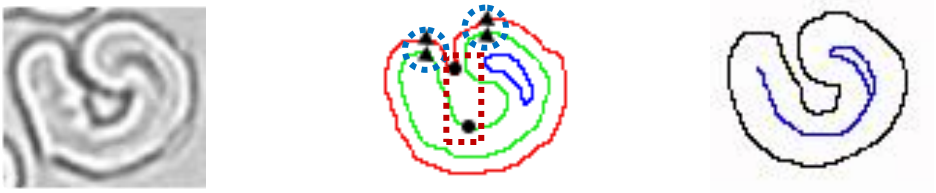

(a) (b) (c)

Figure 3.11 (a) An original self-rolling cross-section. (b) Detected outer and inner contours with concave and convex points. (c) Refined inner contour.

As of a contaminated cross-section, the only failed criterion is that more convex points are detected on the outer contour, and they are unable to find paired points on the inner contour, as seen the points in the red box in figure 3.12(b). Assume that c_o has M points, i.e., $c_o = \{P_0, P_1, \dots, P_{M-1}\}$ and c_i has K points, i.e., $c_i = \{p_0, p_1, \dots, p_{K-1}\}$. In order to trim the tail, the unpaired points on c_o are denoted as $\{uP_1, uP_2, \dots, uP_{N-1}\}$, $N < M$, and they are arranged with counter-clock wise. By picking every two points by order, we can assume that tails may exist between the chosen points. The tail candidates should within the set $T_{candidiates}$, i.e. $T_{candidiates} = \{(uP_1, uP_2), (uP_2, uP_3), \dots, (uP_{N-2}, uP_{N-1})\}$. (uP_{N-2}, uP_{N-1}) is a subset in $T_{candidiates}$, which represents all the contour points from uP_{N-2} to uP_{N-1}. An corresponding points set on the inner contour T_{c_i} can be found, i.e. $T_{c_i} = \{(up_1, up_2), (up_2, up_3), \dots, (up_{N-2}, up_{N-1})\}$. By calculating the average distance between points of each subset in $T_{candidiates}$ and T_{c_i}, a Euclidean Distance set $T_{distance} = \{Avg\_Dis_{1\_2}, Avg\_Dis_{2\_3}, \dots, Avg\_Dis_{N-2\_N-1}\}$ can be generated. In this research, the normal average distance between c_i and c_o is about 5 pixels. If a $Avg\_Dis_{N-2\_N-1} > 5$, the corresponding subset in $T_{candidiates}$ is considered with a tail.

By simply moving the points in the corresponding subset in T_{c_i} toward the outer contour direction with Avg_Dis_{normal} pixels, the original tail points are substituted by the moved inner contour points, as seen figure 3.12(c).

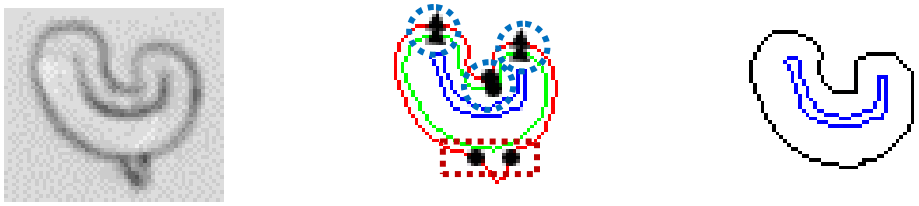

(a) (b) (c)

Figure 3.12 (a) An original contaminated cross-section. (b) Detected outer and inner contours with concave and convex points. (c) Refined outer contour.

3.5.4 Splitting Adhered Cross-sections

As shown in figure 3.3(c), adhered cross-sections generated one outer contour, c_o, and multiple inner contours, C_i. Although we can utilized the unpaired concave points on c_o to determine valid splitting lines using equation 3.22, the method was reported very time consuming by [22]. The same as the self-rolling case, we can simply use the inner contours information. We firstly determine whether each detected c_i^N has normal cross-section shape according to the *TAR* result. It is found that a normal cross-section has less than three convex points and less than two concave points. If an inner contour meets the criteria, the c_i^N area will be dilated for 2 pixels, as shown in figure 3.13. Each of three contours in figure 3.13 has two convex and one concave points which demonstrate a correct cross-section shape.

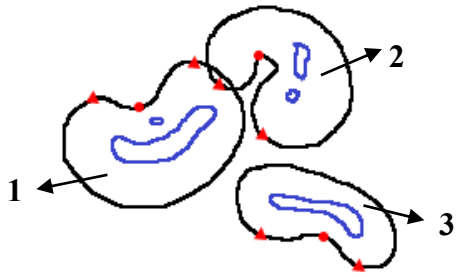

Figure 3.13 Splitted adhering cross-sections.

3.6 REFINING LUMEN CONTOUR

In a cross-section image, often some cross-sections do not possess visible entire lumens, such as immature fibers with totally collapsed lumens, fibers with low contrasts, or fibers only existed partial lumens. In figure 3.13, only fiber 3 is detected an entire lumen; fiber 1 contains two lumen areas, and obviously the smaller one should be considered as noise; only a part of lumen is detected in fiber 2. If no further processing performs, lumen area of fiber 1 will be overestimated, and fiber 2's lumen area will be underestimated.

By evaluating cross-sections geometry, a lumen should be situated in the center of the fiber. Therefore, a correct lumen area should pass over the fiber skeleton, i.e. the middle axis of the fiber. With a refined cross-section, its skeletons can be extracted in an iterative process [13]. Figure 3.14(a) shows the skeleton results of cross-sections in figure 3.13. Let c_s be the calculated skeleton points. The lumen refining processing can be performed as following,

If $Region(c_s) \cap Region(c_l) = \emptyset$, c_s will be used as the lumen contour of the cross-section.

Otherwise, c_s and c_l will be filtered to form a new set of lumen contour c_l' by following operations,

$$c_l' = \{c|(c \in c_l\ ) \wedge (Region(c_s) \cap Region(c_l) \neq \emptyset)\}, \quad (3.25)$$

As seen in figure 3.14(b), the refined lumen region defined by c_l' can be found as,

$$Region(c_l') = (\bigcup_{c \in c_l'} Region(c)) \cup Region(c_l). \quad (3.26)$$

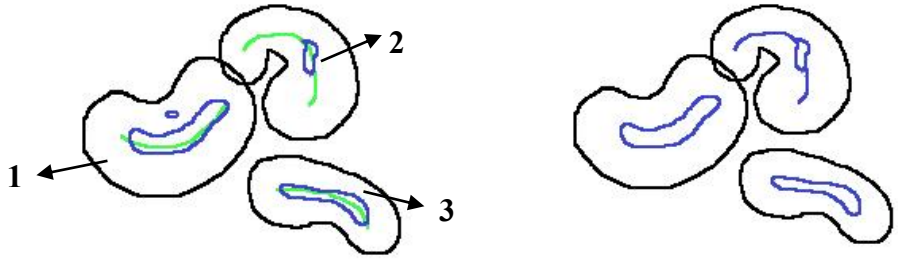

(a) (b)

Figure 3.14 (a) Cross-sections with skeleton information. (b) Lumens refined cross-sections.

Chapter 4: Cotton Fiber Cross-section Detection Algorithm Evaluation

Microsoft Visual Studio 2010 was the development tool to implement the fiber cross-section detection algorithm under Windows 8.1 platform. All testing and developing processes were under a PC equipped by Intel quad core at 2.66 GHz with 4 GB RAM. 7 of 104 cotton varieties were randomly picked out for system performance evaluation.

4.1 Algorithm Results Accuracy Discussion

The manual interpretation (MI) included the automatic detection of cross-sections with our software and human's on-screen corrections for miss- or wrongly-identified cross-sections was introduced. The MI was used as the ground truth to evaluate result accuracy of the proposed algorithm. Figure 4.1(a) displays an example image of cotton cross-sections with a selected ROI for a clearer demonstration with larger contours. We visually compared cross-section detection results between the previous algorithm (PA) (figure 4.1(b)) and the current algorithm (CA) (figure 4.1(c)). From figure 4.1(c), most detection defects in figure 4.1(b) were corrected by current algorithm. Figure 4.1(d) shows the maturity (θ) distributions of one of the selected 7 cottons that obtained by using the CA and the MI. The two distributions are highly correlated (R^2 =0.985). Table 4.1 lists the fiber maturity distribution correlations of the 7 cottons. The higher correlation demonstrates that cotton fiber maturity evaluation with the proposed algorithm has similar results with human visual analysis.

Table 4.1 The correlations of CA and MI evaluated maturity distribution of 7 cottons.

Cotton	1	2	3	4	5	6	7
Correlation	0.985	0.978	0.954	0.987	0.984	0.968	0.961

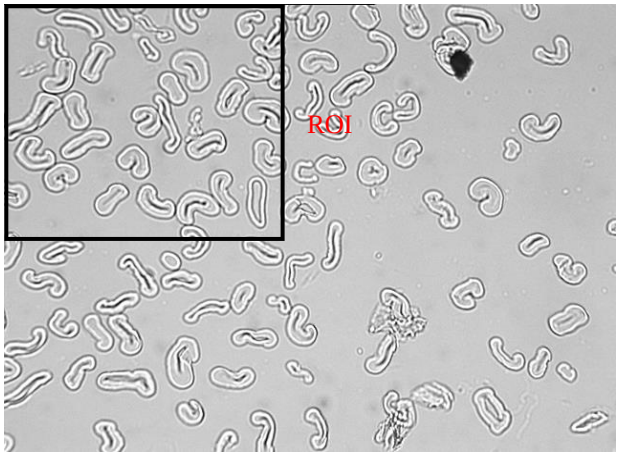

(a)

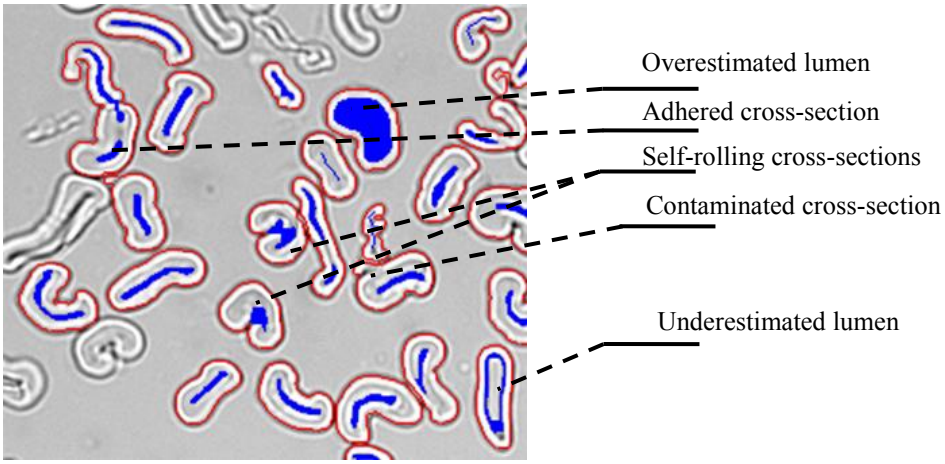

(b) Detection result based on previous algorithm.

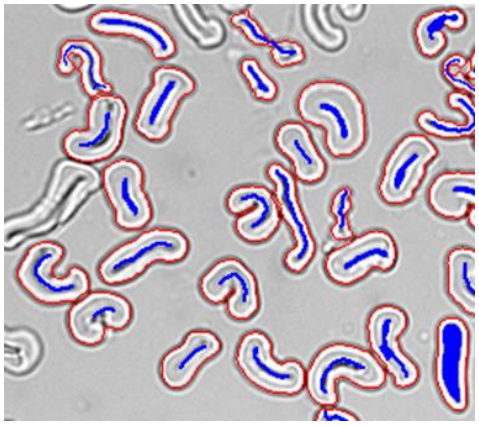

(c) Detection result with current algorithm.

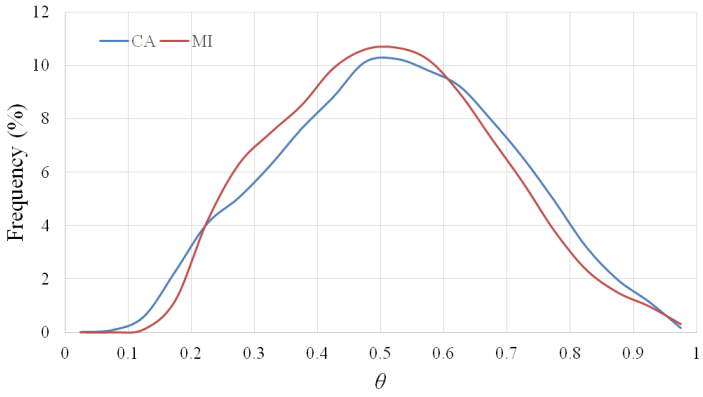

(d) Maturity (θ) distributions of the CA and the MI.

Figure 4.1 An example of cross-sections detection result and accuracy evaluation.

4.2 ALGORITHM EFFICIENCY

There are seven major steps of the proposed algorithm, including *locating contours* (*LC*), *triangle-area representation* (*TAR*), *splitting inner contours* (*SIC*), *merging inner contours* (*MIC*), *refining outer contours* (*ROC*), *Splitting adhered cross-sections* (*SAC*), and *refining lumen contour* (*RLC*). By accumulating the time consumption of each step, a time consumption chart of 7 cottons is formed as shown in figure 4.2. The algorithm processing time of the evaluated seven cottons are within 60 to 90 seconds. Time variance is because different numbers of cross-sections of each cotton were detected. Among the seven steps, because each cross-section need to be performed under *LC* and *RLC*, these two steps occupy the majority portion of the entire processing time. *ROC* is the third time consumption of the entire evaluating, which indicates self-rolling and contaminated cross-sections exists a lot in each cotton.

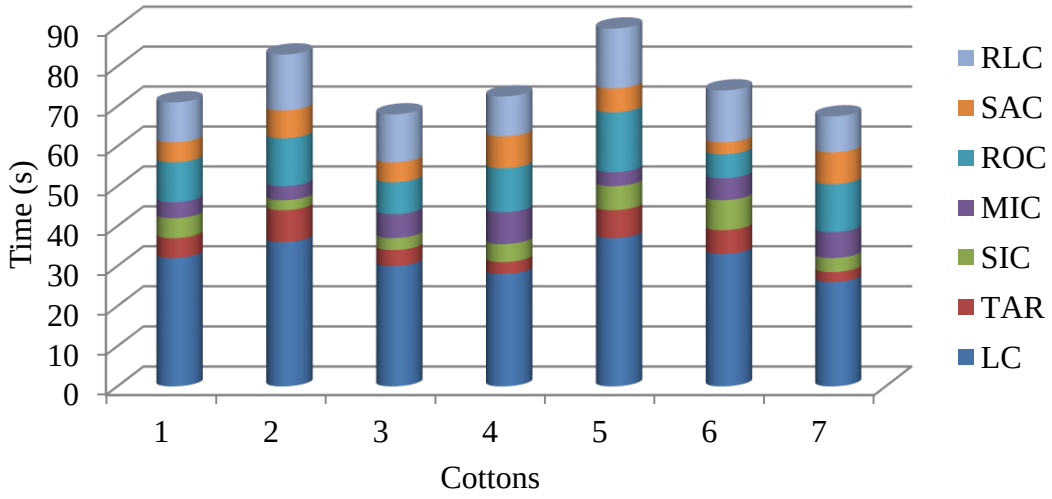

Figure 4.2 Time consumption in major steps of the proposed algorithm.

4.3 ERROR ANALYSIS

The error analysis of cotton fiber maturity is performed by comparing maturity measurements of 7 cottons from the proposed algorithm to those from the MI. Figure 4.3 illustrates the average errors and error uncertainties of the maturity data measured by the CA and the PA. The average errors and uncertainties of CA is about 50% smaller than those of PA. This also demonstrates that the CA increase the accuracy of cross-sections detection.

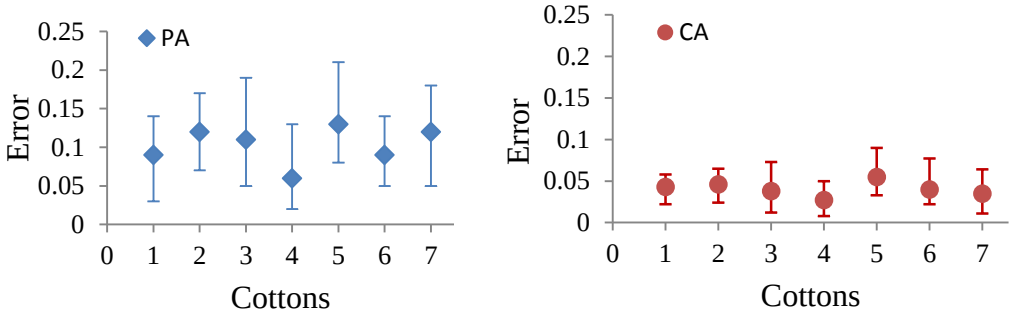

Figure 4.3 Error in calculating maturity (a) with PA, and (b) based on CA.

Chapter 5: Data Analysis and Discussion

5.1 Sample collection and Distribution Parameters

A total of 15473 fiber cross-sectional images from 104 image sets that was provided by the Fiber and Biopolymer Research Institute (FBRI) of Texas Tech University were examined via the new FIAS system. The 104 image sets represented 104 cotton bales from USA, Egypt, Uzbekistan, Pakistan, Cameroon, Syria, Benin, and Australia. For each bale, about 30kg cotton were taken out and divided into eight sub-samples. A minimum of 500 cross-sections were imaged via a digital microscope per sub-sample.

After investigated the pervious fiber maturity study, we found that only the mean (M_θ) was not sufficient to describe the fiber maturity distribution because it just represents the central tendency and the variability of the distribution. More descriptive parameters including standard deviation (SD_θ), skewness (S_θ) and kurtosis (K_θ) were introduced in this study.

Skewness indicates the "symmetry" of a distribution. The skewness of a normal (bell-shaped) distribution is zero. A positive skew presents a long tail on the left side of a bell while a right-skewed distribution is with a negative value.

Kurtosis is another descriptor of the shape of a distribution. A low kurtosis presents a distribution with more rounded peak and short, thinner tails. A needle shaped distribution always has a higher kurtosis.

5.2 Fiber contents of 104 Cottons

Fiber contents describe the dead, immature and mature percentage according to average cross-sections maturity θ in each sample, as seen in table 5.1. The immature fibers take 43% (cotton 3140) to 65% (cotton 3097) of the total fibers in these cottons,

the dead fiber contents vary from 6% (cotton 3074) to 48% (cotton 3089), and the mature fiber contents vary from 7% (cotton 3085) to 50% (cotton 3140). In each cotton, immature fibers are the main body of the fibers. Averagely, the dead fiber content and the mature fiber content are 17.7% and 23.7%, respectively.

Table 5.1 Dead, Immature and Mature Fiber Contents.

Cotton	Dead (%)	Immature (%)	Mature (%)	Cotton	Dead (%)	Immature (%)	Mature (%)
2996	11.495	63.806	24.698	3145	15.634	62.764	21.602
2999	23.112	62.232	14.656	3146	9.900	59.072	31.028
3008	21.007	61.262	17.731	3147	11.088	54.199	34.712
3009	11.100	63.996	24.903	3150	13.795	61.568	24.638
3016	15.714	62.480	21.806	3151	16.640	60.765	22.594
3074	6.335	56.706	36.958	3152	18.207	58.826	22.967
3075	28.644	58.755	12.600	3153	17.471	61.186	21.344
2684	15.013	59.505	25.482	3154	10.397	55.688	33.915
2792	8.801	50.581	40.618	3155	6.978	54.740	38.281
2888	9.779	49.902	40.318	3156	9.256	55.598	35.146
2952	14.563	54.824	30.613	3157	22.696	56.945	20.359
3004	14.535	52.175	33.290	3158	17.669	59.873	22.458
3022	12.975	61.099	25.926	3159	22.765	54.728	22.507
3029	13.681	61.225	25.094	3160	19.705	60.401	19.894
3030	21.306	62.626	16.068	3161	18.478	60.419	21.103
3033	18.026	59.128	22.847	3162	16.047	60.807	23.146
3035	25.619	60.433	13.948	3165	16.072	61.257	22.672
3038	16.608	64.654	18.738	3166	22.026	64.141	13.833
3039	20.380	57.697	21.923	3167	11.655	59.493	28.852
3042	13.590	61.244	25.166	3168	19.710	59.871	20.419
3043	19.174	61.311	19.515	3169	16.421	62.541	21.039
3044	19.722	59.695	20.583	3170	29.187	59.406	11.408
3045	11.248	54.303	34.449	3171	21.381	58.669	19.950
3046	12.864	57.054	30.082	3172	16.589	58.228	25.183
3051	25.332	60.523	14.145	3173	18.439	59.057	22.504
3054	17.372	58.332	24.296	3174	12.545	60.537	26.918
3055	17.059	63.067	19.874	3175	13.510	59.393	27.097
3056	22.071	60.962	16.967	3176	13.625	59.749	26.625
3057	25.108	60.987	13.905	3177	15.159	57.363	27.478
3068	19.375	58.691	21.935	3178	14.878	61.227	23.896
3081	13.709	61.416	24.874	3179	18.489	61.280	20.231
3089	47.818	44.692	7.490	3180	19.452	60.839	19.709

Table 5.1 Continued…

3096	34.006	56.225	9.769
3097	20.095	64.661	15.244
3104	26.992	59.644	13.364
3106	14.251	63.667	22.083
3107	8.794	63.875	27.330
3112	11.416	62.486	26.097
3115	37.956	53.957	8.086
3116	47.463	45.130	7.407
3117	31.109	54.531	14.360
3119	21.840	59.906	18.254
3122	12.895	57.074	30.031
3123	18.974	59.858	21.168
3129	43.200	47.878	8.922
3132	21.100	59.495	19.405
3138	22.944	61.753	15.302
3140	6.476	43.839	49.685
3141	6.589	64.196	29.215
3142	8.900	50.486	40.614
3143	8.101	51.438	40.462
3144	20.275	60.908	18.817
Average	17.673	58.596	23.731
Min	6.335	43.839	7.407
Max	47.818	64.661	49.685

3181	14.659	56.119	29.222
3182	13.432	59.653	26.915
3183	15.903	61.663	22.433
3184	16.371	56.472	27.157
3185	15.526	58.824	25.650
3186	15.508	57.764	26.729
3187	24.182	60.233	15.586
3188	19.477	61.140	19.383
3189	20.710	61.493	17.797
3190	15.131	56.440	28.429
3191	17.296	57.519	25.185
3192	16.504	61.128	22.368
3193	17.308	60.961	21.731
3194	18.972	61.773	19.255
3195	20.149	61.702	18.148
3196	9.514	55.387	35.099
3212	8.063	50.147	41.790
3214	17.497	57.454	25.050
3215	9.953	52.598	37.449
4409	9.458	58.487	32.055

5.3 MATURITY DISTRIBUTIONS OF 104 COTTONS

After scrutinizing the maturity distributions of the 104 reference cottons listed in figure 5.1, we found that cottons had very diversified maturity distributions ranging from highly right-skewed (positive) to highly-left skewed (negative). And the majority of the 104 cotton fiber distributions were not normal. In this study, skewness was the first principal parameter that could depict the normality of distributions. In table 5.2, the normality of distributions was classified into five groups by the skewness values. $S_\theta \geq 0.3$ indicated a severely right-skewed distribution that can be recognized that a large number dead fibers were detected in the sample. A slightly positive S_θ within rang [0.1, 0.3) represents more immature fibers. An approximately normal distribution with S_θ [-0.1, 0.1)

denoted most immature and mature fibers were found. We also defined that a sample with mostly mature fibers had S_θ within range [-0.3, - 0.1). If S_θ goes beyond -0.3, a conclusion of the majority of highly mature fibers in the sample will be made.

Table 5.2 Maturity Classification by Skewness.

Class	Skewness (S_θ)	Shape	Main Fiber Content
I	$S_\theta \geq 0.3$	Severely right-skewed	Dead fibers
II	$0.1 \leq S_\theta < 0.3$	Right-skewed	Immature fibers
III	$-0.1 \leq S_\theta < 0.1$	Approximately normal	Immature and mature fibers
IV	$-0.3 \leq S_\theta < -0.1$	Left-skewed	Mature fibers
V	$S_\theta < -0.3$	Severely left-skewed	Highly mature fibers

Of the 104 reference cottons, there are 20 cottons classified as class I, 39 as class II, 30 as class III, 14 as class IV, and 1 as class V. This means that there are about 20% cottons in this set that contain high levels of dead fibers, only 14% contain high levels of mature fibers, and the maturity levels of most cottons are within the low-moderate range, as seen in table 5.3.

Table 5.3 Maturity classifications of the 104-Reference Cottons.

Class	Distribution	Maturity	Number	Cotton
I	Severely right-skewed	Very low	20	2999 3008 3075 3030 3035 3051 3056 3057 3089 3096 3104 3115 3116 3117 3129 3138 3166 3170 3187 3195
II	Right-skewed	Low	39	3016 3033 3038 3039 3043 3044 3055 3068 3097 3119 3123 3132 3144 3145 3150 3151 3152 3153 3157 3158 3159 3160 3161 3162 3165 3168 3169 3171 3172 3173 3179 3180 3188 3189 3191 3192 3193 3194 3214
III	Approximately normal	Moderate	30	2996 3009 2684 2952 3004 3022 3029 3042 3046 3054 3081 3106 3107 3112 3122 3141 3146 3167 3174 3175 3176 3177 3178 3181 3182 3183 3184 3185 3186 3190
IV	Left-skewed	High	14	3074 2792 2888 3045 3142 3143 3147 3154 3155 3156 3196 3212 3215 4409
V	Severely left-skewed	Very high	1	3140

Compared with the conclusion made in section 5.2, we found that using the distribution shape as a cotton maturity descriptor provided more information and gave a more reasonable result. For example, Cotton 2996 and 2999, based on the fiber contents results, it is hard to distinguish these two sample. A general conclusion would be both of them should come from the same source. However, when looking at the distribution shapes of two cottons, the difference is apparently. Cotton 2999 showed a very low maturity while cotton 2996 had a moderate maturity.

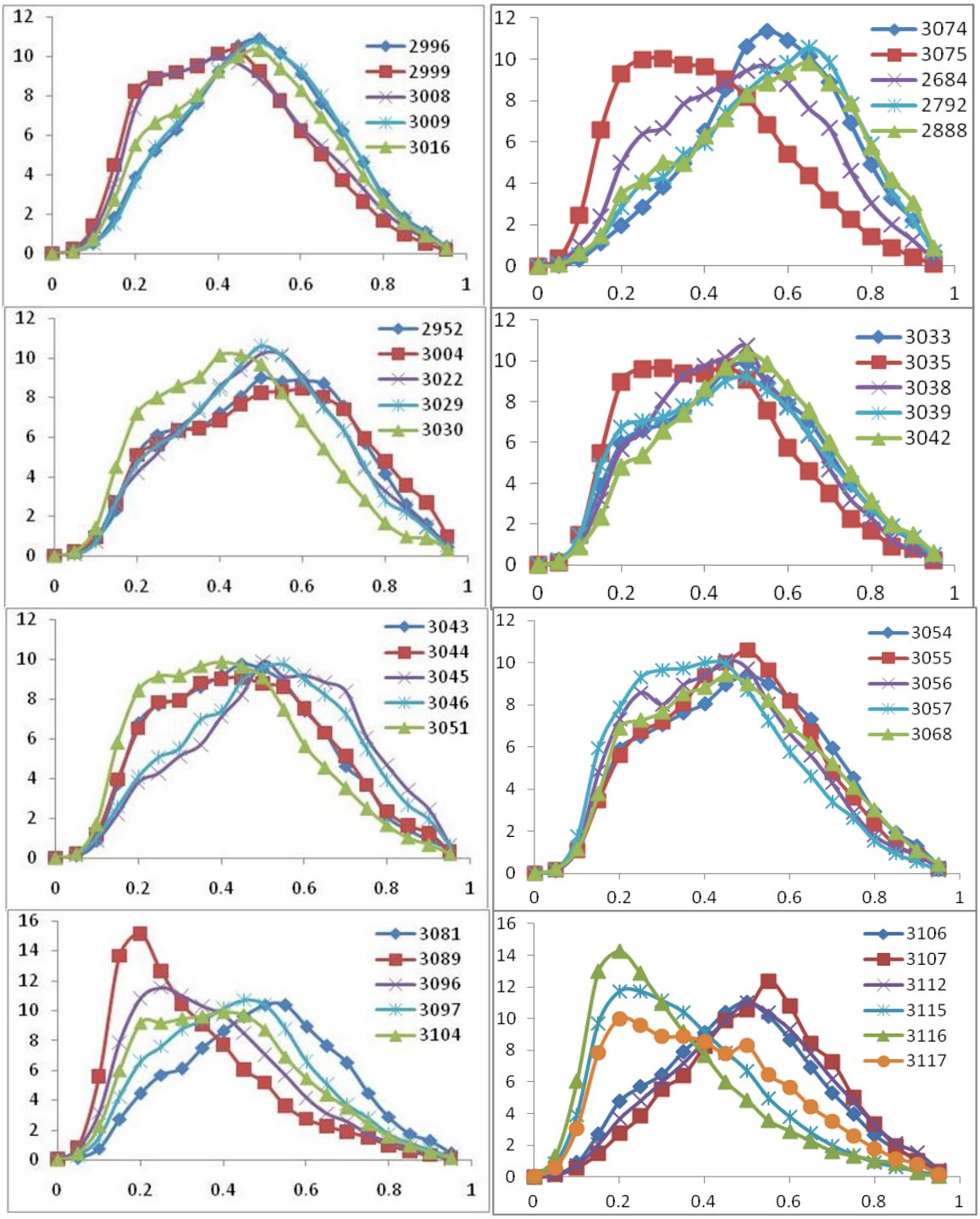

Figure 5.1 Cotton maturity distributions of the 104 reference cottons.

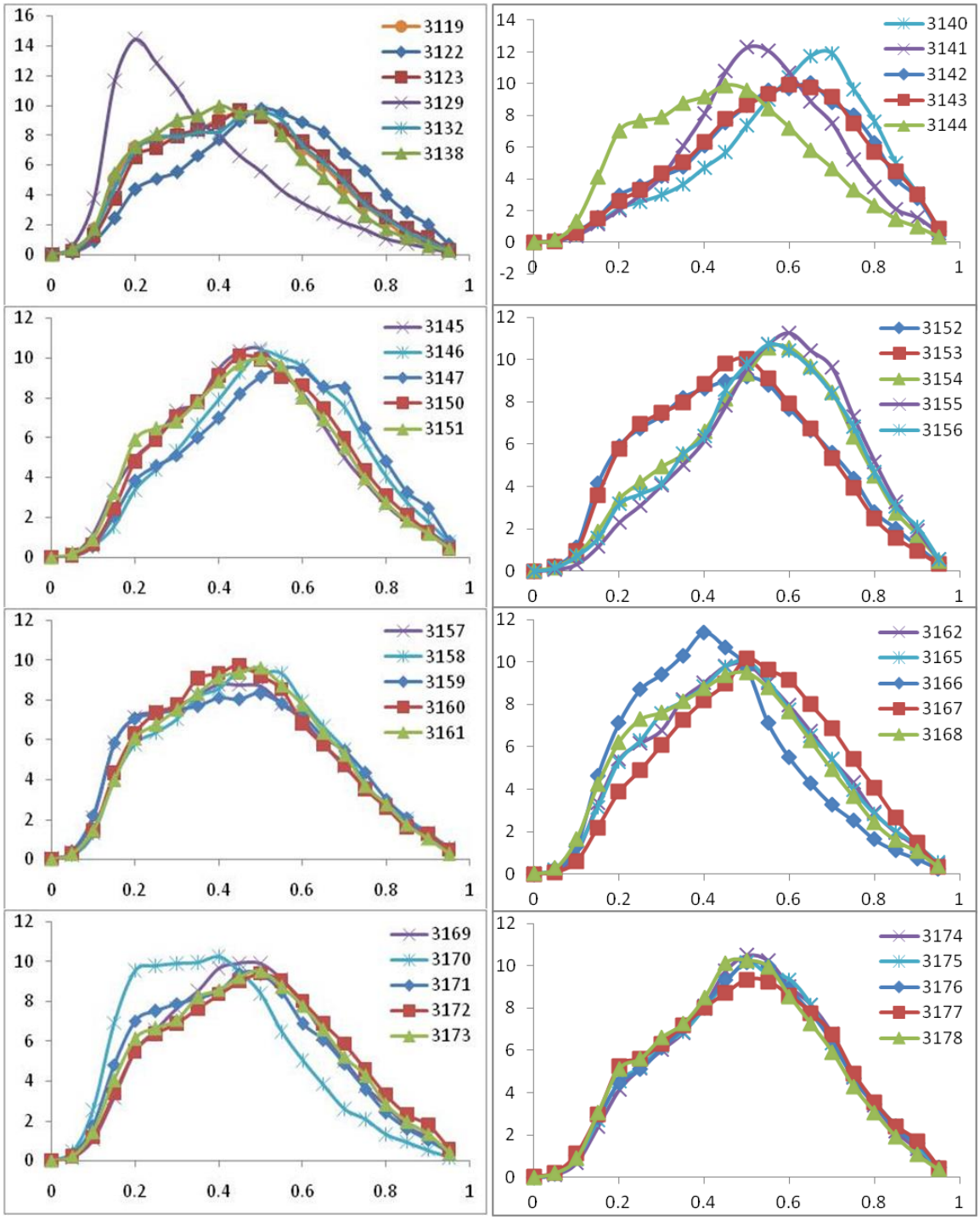

Figure 5.1 Continued…

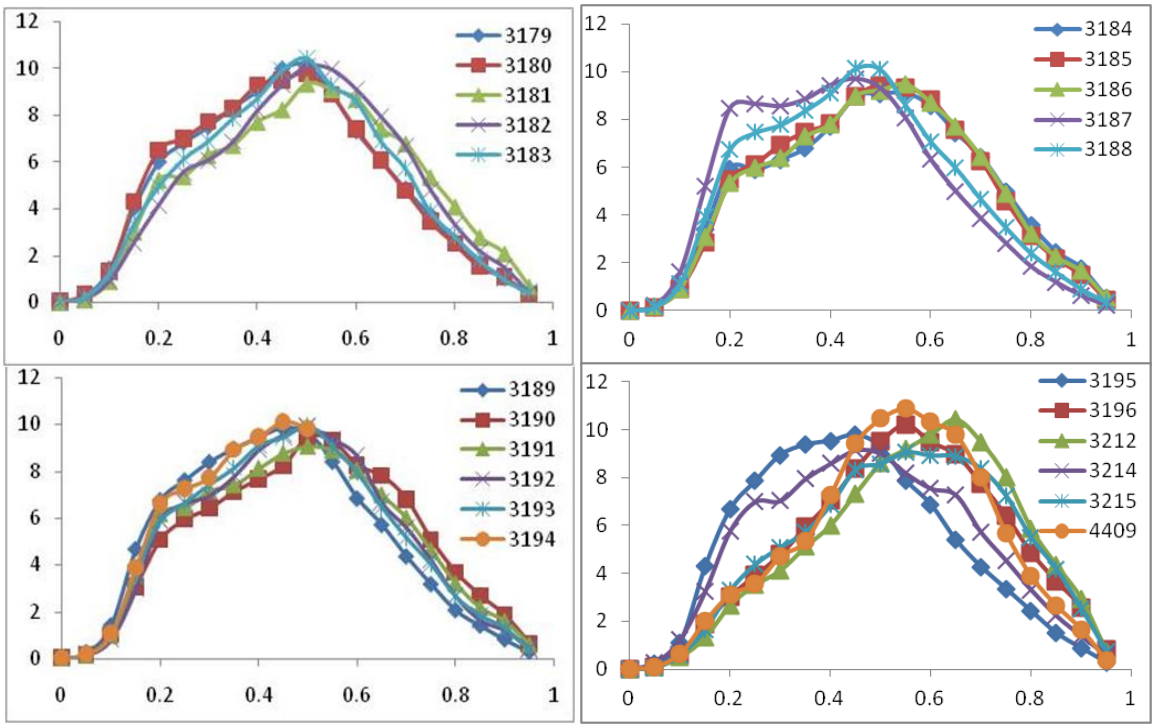

Figure 5.1 Continued…

5.4 AFIS-FAIS COMPARISON

The raw AFIS maturity data of the 104 cottons were provided by Dr. Eric Hequet at the Fiber and Biopolymer Research Institute (FBRI) of TTU. Table 5.4 lists the four cotton maturity descriptors for both AFIS and FAIS of the 104 cottons. Compared the correlation of the 4 descriptive parameters, AFIS and FIAS have good correlations only in mean θ ($R^2 = 0.791$), as seen in figure 5.2. The standard deviation value of each cotton in FIAS larger than the value of AFIS indicates that the detected cross-section in each FIAS sample is spread out over a wider range of values. This demonstrates that the new algorithm of FIAS has the ability to detect more different types of cross-sections. The skewness range of FIAS is wider than the range of AFIS proved that the 104 cottons should be from different sources and their qualities are more distinguishable with FIAS

detection results. The Kurtosis values in AFIS are all negative that indicated the fiber contents analyzed by AFIS are very concentrated in a wider range. However, the Kurtosis of the 104 cotton via FIAS do have some positive values that meant those samples might have a certain fiber content with extreme number.

Table 5.4 AFIS and FAIS cotton maturity descriptive parameters.

Cotton	Mean		SD		Skewness		Kurtosis	
	AFIS	FIAS	AFIS	FIAS	AFIS	FIAS	AFIS	FIAS
2996	0.510	0.524	0.150	0.175	0.004	0.069	-0.338	-0.540
2999	0.454	0.451	0.144	0.177	0.155	0.349	-0.307	-0.483
3008	0.480	0.467	0.153	0.182	0.114	0.360	-0.413	-0.542
3009	0.522	0.525	0.161	0.174	0.031	0.064	-0.398	-0.552
3016	0.485	0.501	0.148	0.180	0.096	0.131	-0.332	-0.625
3074	0.538	0.585	0.156	0.174	-0.067	-0.184	-0.317	-0.383
3075	0.454	0.426	0.144	0.180	0.205	0.438	-0.271	-0.453
2684	0.501	0.515	0.165	0.187	0.053	0.042	-0.495	-0.696
2792	0.530	0.585	0.165	0.187	-0.048	-0.277	-0.436	-0.617
2888	0.522	0.583	0.167	0.194	-0.006	-0.226	-0.438	-0.712
2952	0.509	0.534	0.165	0.194	0.028	-0.037	-0.471	-0.815
3004	0.506	0.545	0.171	0.205	0.080	-0.021	-0.492	-0.859
3022	0.494	0.525	0.146	0.185	0.043	0.061	-0.293	-0.595
3029	0.509	0.520	0.151	0.183	0.038	0.060	-0.277	-0.609
3030	0.494	0.463	0.149	0.180	0.060	0.302	-0.335	-0.463
3033	0.496	0.498	0.156	0.191	0.109	0.118	-0.321	-0.668
3035	0.476	0.443	0.142	0.180	0.065	0.435	-0.288	-0.411
3038	0.503	0.485	0.149	0.177	0.031	0.194	-0.314	-0.514
3039	0.500	0.488	0.153	0.195	0.118	0.177	-0.282	-0.715
3042	0.516	0.520	0.161	0.185	0.052	0.078	-0.359	-0.571
3043	0.485	0.482	0.152	0.184	0.112	0.247	-0.320	-0.599
3044	0.491	0.483	0.154	0.189	0.119	0.236	-0.327	-0.653
3045	0.520	0.559	0.166	0.193	0.077	-0.128	-0.392	-0.666
3046	0.524	0.539	0.162	0.192	0.045	-0.038	-0.360	-0.664
3051	0.480	0.443	0.142	0.181	0.053	0.403	-0.311	-0.439
3054	0.495	0.504	0.156	0.192	0.089	0.091	-0.323	-0.738
3055	0.500	0.491	0.145	0.180	0.020	0.129	-0.295	-0.572
3056	0.479	0.465	0.146	0.183	0.125	0.308	-0.267	-0.523
3057	0.466	0.441	0.140	0.179	0.131	0.395	-0.270	-0.455
3068	0.485	0.489	0.153	0.192	0.117	0.229	-0.335	-0.691
3081	0.499	0.519	0.152	0.182	0.080	0.033	-0.310	-0.589
3089	0.439	0.351	0.135	0.174	0.171	0.949	-0.283	0.424

Table 5.4 Continued…

3096	0.456	0.399	0.139	0.175	0.139	0.611	-0.294	-0.141
3097	0.486	0.463	0.147	0.176	0.101	0.278	-0.312	-0.418
3104	0.491	0.434	0.143	0.180	0.033	0.407	-0.308	-0.453
3106	0.506	0.508	0.146	0.180	-0.014	0.093	-0.296	-0.502
3107	0.515	0.544	0.149	0.171	0.002	-0.094	-0.313	-0.408
3112	0.509	0.531	0.149	0.180	0.011	0.034	-0.319	-0.520
3115	0.449	0.380	0.137	0.173	0.157	0.679	-0.290	0.014
3116	0.421	0.350	0.129	0.175	0.201	0.941	-0.230	0.446
3117	0.448	0.427	0.141	0.192	0.193	0.440	-0.278	-0.557
3119	0.471	0.469	0.144	0.187	0.097	0.223	-0.316	-0.634
3122	0.521	0.540	0.166	0.192	0.052	-0.017	-0.404	-0.679
3123	0.478	0.487	0.154	0.189	0.170	0.194	-0.303	-0.667
3129	0.448	0.371	0.137	0.178	0.170	0.860	-0.270	0.163
3132	0.486	0.477	0.157	0.189	0.136	0.195	-0.382	-0.679
3138	0.482	0.454	0.143	0.182	0.041	0.313	-0.351	-0.488
3140	0.550	0.623	0.175	0.181	-0.040	-0.525	-0.430	-0.245
3141	0.528	0.559	0.151	0.166	-0.034	-0.032	-0.304	-0.250
3142	0.506	0.587	0.163	0.190	0.041	-0.278	-0.433	-0.588
3143	0.541	0.589	0.163	0.189	-0.008	-0.239	-0.323	-0.584
3144	0.476	0.476	0.152	0.186	0.127	0.254	-0.366	-0.594
3145	0.495	0.501	0.157	0.185	0.077	0.162	-0.395	-0.501
3146	0.504	0.552	0.158	0.183	0.057	-0.026	-0.394	-0.588
3147	0.495	0.561	0.163	0.192	0.131	-0.108	-0.398	-0.712
3150	0.485	0.515	0.151	0.183	0.122	0.118	-0.318	-0.637
3151	0.515	0.502	0.157	0.186	0.032	0.132	-0.352	-0.620
3152	0.506	0.496	0.157	0.192	0.044	0.150	-0.376	-0.713
3153	0.505	0.494	0.155	0.185	0.058	0.148	-0.368	-0.638
3154	0.524	0.560	0.160	0.185	0.044	-0.208	-0.371	-0.556
3151	0.515	0.502	0.157	0.186	0.032	0.132	-0.352	-0.620
3152	0.506	0.496	0.157	0.192	0.044	0.150	-0.376	-0.713
3153	0.505	0.494	0.155	0.185	0.058	0.148	-0.368	-0.638
3154	0.524	0.560	0.160	0.185	0.044	-0.208	-0.371	-0.556
3155	0.533	0.586	0.162	0.175	0.008	-0.258	-0.383	-0.436
3156	0.523	0.570	0.161	0.183	0.048	-0.213	-0.384	-0.486
3157	0.483	0.474	0.151	0.198	0.086	0.257	-0.350	-0.686
3158	0.491	0.498	0.151	0.191	0.078	0.156	-0.346	-0.630
3159	0.466	0.481	0.142	0.203	0.153	0.180	-0.243	-0.827
3160	0.496	0.481	0.149	0.190	0.054	0.263	-0.318	-0.568
3161	0.498	0.489	0.152	0.189	0.096	0.161	-0.325	-0.658
3162	0.497	0.504	0.149	0.188	0.054	0.145	-0.318	-0.623
3165	0.478	0.502	0.147	0.188	0.125	0.172	-0.316	-0.592
3166	0.471	0.449	0.146	0.175	0.123	0.441	-0.364	-0.244

Table 5.4 Continued…

3167	0.501	0.537	0.145	0.185	0.050	-0.005	-0.294	-0.683
3168	0.480	0.484	0.148	0.190	0.114	0.181	-0.327	-0.639
3169	0.490	0.495	0.145	0.184	0.066	0.197	-0.313	-0.566
3170	0.472	0.420	0.146	0.178	0.118	0.494	-0.354	-0.269
3171	0.475	0.476	0.150	0.192	0.129	0.225	-0.342	-0.655
3172	0.478	0.511	0.149	0.195	0.140	0.124	-0.325	-0.703
3175	0.500	0.527	0.149	0.187	0.033	-0.001	-0.308	-0.640
3176	0.505	0.525	0.149	0.188	0.012	0.012	-0.311	-0.618
3177	0.503	0.522	0.162	0.193	0.126	0.022	-0.370	-0.725
3178	0.504	0.512	0.147	0.184	0.016	0.053	-0.280	-0.612
3179	0.501	0.487	0.150	0.187	0.028	0.186	-0.340	-0.592
3180	0.499	0.482	0.148	0.188	0.038	0.204	-0.311	-0.600
3181	0.498	0.531	0.158	0.197	0.092	0.020	-0.359	-0.766
3182	0.501	0.527	0.150	0.186	0.021	0.003	-0.315	-0.624
3183	0.495	0.503	0.146	0.185	0.043	0.081	-0.305	-0.601
3184	0.493	0.519	0.160	0.196	0.132	0.047	-0.357	-0.763
3185	0.494	0.515	0.158	0.190	0.122	0.072	-0.357	-0.708
3186	0.498	0.520	0.160	0.192	0.116	0.048	-0.377	-0.712
3187	0.478	0.453	0.153	0.183	0.133	0.333	-0.370	-0.541
3188	0.485	0.481	0.147	0.186	0.078	0.238	-0.346	-0.588
3189	0.482	0.470	0.145	0.184	0.076	0.262	-0.304	-0.562
3190	0.500	0.526	0.162	0.195	0.122	0.039	-0.365	-0.751
3191	0.486	0.508	0.159	0.195	0.155	0.128	-0.372	-0.746
3192	0.491	0.502	0.154	0.185	0.123	0.134	-0.331	-0.635
3193	0.501	0.496	0.150	0.188	0.043	0.174	-0.344	-0.627
3194	0.492	0.481	0.145	0.185	0.049	0.251	-0.307	-0.573
3195	0.488	0.472	0.146	0.185	0.038	0.312	-0.335	-0.556
3196	0.496	0.568	0.154	0.189	0.087	-0.113	-0.375	-0.613
3212	0.524	0.592	0.167	0.187	0.082	-0.275	-0.392	-0.592
3214	0.492	0.505	0.159	0.195	0.140	0.146	-0.357	-0.732
3215	0.511	0.572	0.165	0.193	0.111	-0.142	-0.403	-0.739
4409	0.520	0.557	0.154	0.179	0.039	-0.174	-0.287	-0.449
Max	**0.550**	**0.623**	**0.175**	**0.205**	**0.205**	**0.949**	**-0.230**	**0.446**
Min	**0.421**	**0.350**	**0.129**	**0.166**	**-0.067**	**-0.525**	**-0.495**	**-0.859**
R^2	**0.791**		**0.206**		**0.374**		**0.147**	

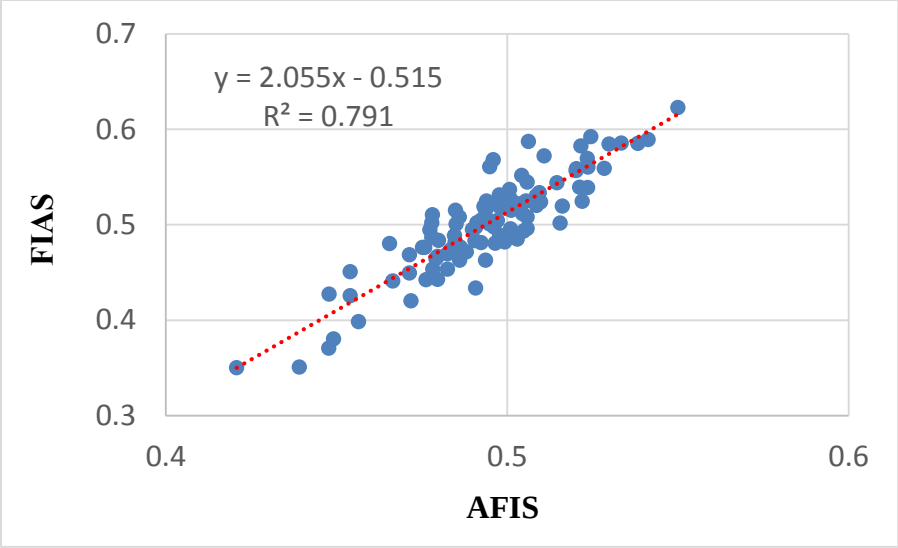

Figure 5.2 The correlation of the mean $\theta\,(M_\theta)$ of the 104 cottons generated by AFIS and FIAS.

At the bottom of table 5.3, the max-min ranges of the four descriptive parameters of the 104 cottons are displayed. We will use the maturity distributions of the cottons with these extreme parameters as examples to show the differences in the maturity distributions between AFIS and FIAS. Figure 5.3 shows the maturity (θ) distributions of cotton 3175 whose absolute skewness value from FIAS is close to zero (-0.001), meaning the FIAS distribution is approximately symmetrical. But since it has a large negative kurtosis (-0.640), this distribution is platykurtic. On the other hand, the AFIS distribution of the same cotton is more similar to a normal distribution, which underestimates mature fibers (the yellow region) but overestimates immature fibers (the green region).

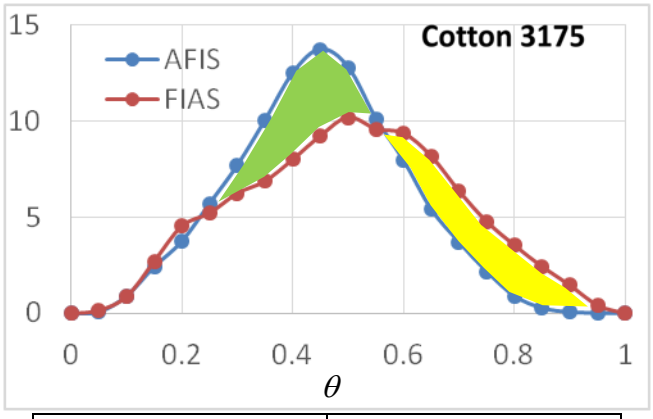

Skewness		Kurtosis	
AFIS	FIAS	AFIS	FIAS
0.033	-0.001	-0.308	-0.640

Figure 5.3 FIAS maturity distribution of cotton 3175 with the lowest absolute skewness.

Figure 5.4 presents the FIAS maturity distribution of a cotton (3140) that has the most negative skewness (left-skewed). The corresponding AFIS maturity distribution of this cotton still looks like a normal distribution (skewness = -0.04), which severely underestimates mature fiber contents for this highly mature cotton sample (the yellow region).

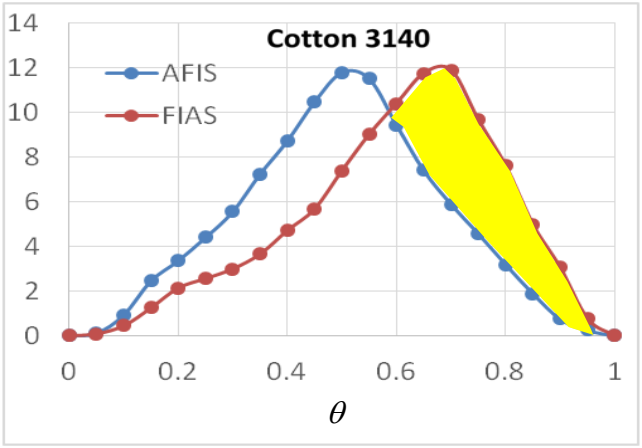

Skewness		Kurtosis	
AFIS	FIAS	AFIS	FIAS
-0.040	-0.525	-0.430	-0.245

Figure 5.4 FIAS maturity distribution of cotton 3140 with the most negative skewness (left-skewed).

Figure 5.5 presents a FIAS maturity distribution (cotton 3089) that has the most positive skewness (0.949), indicating the distribution is severely right-skewed and the main fiber contents in this cotton are dead and immature fibers. But the AFIS distribution of this cotton is still rather normal (skewness = 0.171), underestimating dead fiber contents significantly (the yellow region) for this highly immature cotton.

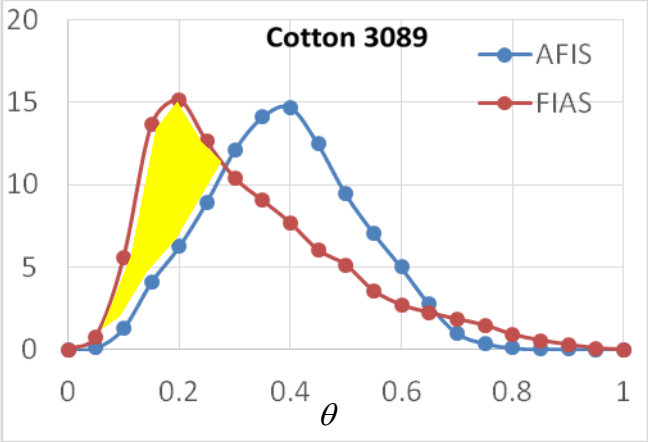

Skewness		Kurtosis	
AFIS	FIAS	AFIS	FIAS
0.171	0.949	-0.283	0.424

Figure 5.5 FIAS maturity distribution of cotton 3089 with the most positive skewness (right-skewed).

Figure 5.6 shows the FIAS maturity distribution of cotton 3004 that has the most negative kurtosis (flat) among the sample set. The distribution has a very flat top, indicating a wide range of maturity distributions. Its AFIS distribution underestimates the mature fiber content.

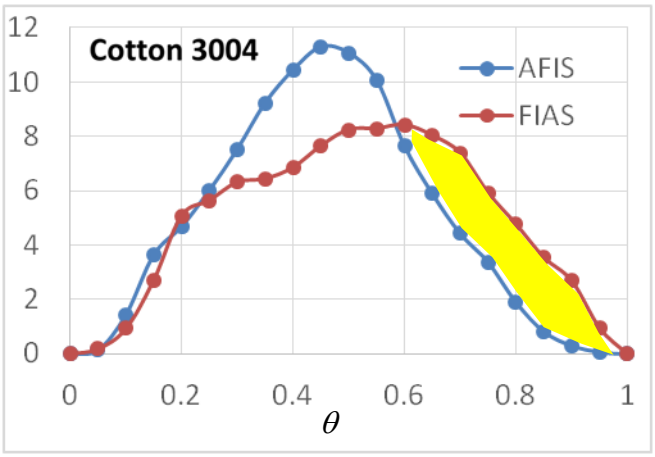

Skewness		Kurtosis	
AFIS	FIAS	AFIS	FIAS
0.080	-0.021	-0.492	-0.859

Figure 5.6 FIAS maturity distribution of cotton 3004 with the most negative kurtosis (flat).

Figure 5.7 shows the FIAS maturity distribution of cotton 3116 that has the both of high positive skewness and kurtosis with a right-skewed and sharp-peak shape. But AFIS distribution again present a mild dead fiber contents, which is significantly less than the FIAS detected dead fibers.

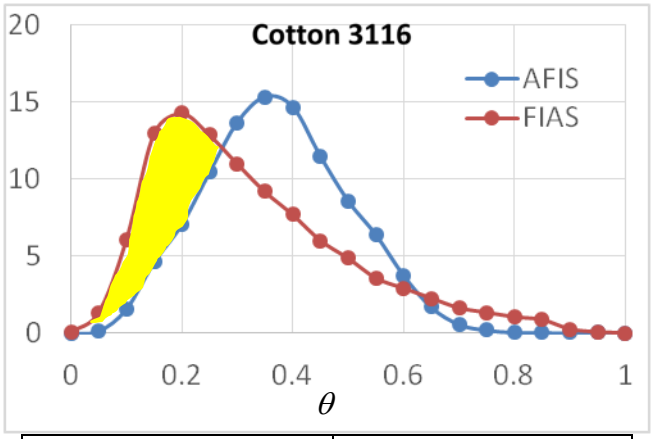

Skewness		Kurtosis	
AFIS	FIAS	AFIS	FIAS
0.201	0.941	-0.230	0.446

Figure 5.7 FIAS maturity distribution of cotton 3116 with both of high positive skewness and kurtosis (right-skewed and sharp).

Using table 5.2 as a reference, we also classified AFIS maturity distribution data into five classes, listed in table 5.5. It can be seen that AFIS can only classify the 104 cottons into two maturity classes: II and III (immature and mature fibers), missing the classifications of cottons containing predominantly dead (class I) and mature (class IV or V) fibers.

Table 5.5 Maturity classifications by AFIS.

Class	Maturity	Number	Cotton
I ($S_\theta \geq 0.3$)	Very low	0	N/A
II ($0.1 \leq S_\theta < 0.3$)	Low	40	2999 3008 3075 3033 3039 3043 3044 3056 3057 3068 3089 3096 3097 3115 3116 3117 3123 3129 3132 3144 3147 3150 3159 3165 3166 3168 3170 3171 3172 3173 3177 3184 3185 3186 3187 3190 3191 3192 3214 3215
III ($-0.1 \leq S_\theta < 0.1$)	Moderate	64	2996 3009 3016 3074 2684 2792 2888 2952 3004 3022 3029 3030 3035 3038 3042 3045 3046 3051 3054 3055 3081 3104 3106 3107 3112 3119 3122 3138 3140 3141 3142 3143 3145 3146 3151 3152 3153 3154 3155 3156 3157 3158 3160 3161 3162 3167 3169 3174 3175 3176 3178 3179 3180 3181 3182 3183 3188 3189 3193 3194 3195 3196 3212 4409
IV ($-0.3 \leq S_\theta < -0.1$)	High	0	N/A
V ($S_\theta < -0.3$)	Very high	0	N/A

By comparing the corresponding AFIS and FIAS maturity distributions, we find that AFIS mature distributions appear to be more normal, less skewed and more concentrated than FIAS distributions; AFIS distributions tend to underestimate the mature fiber contents for highly mature cotton samples and the immature fiber contents for highly immature cotton samples; and the shapes of the two maturity distributions are significantly different even if the mean values of both maturity distributions are close to each other. For cotton fiber quality control based on maturity analysis, AFIS results are not very distinguishable between different samples.

Chapter 6: Conclusions and Future Work

6.1 SUMMARY OF THE THESIS

The purpose of cotton maturity evaluation is to exam cotton bales quality. Cotton scientists have consent that among different cotton maturity measurement methods the fiber cross-section geometric measurement is the most reasonable approach. And digital image analysis on the cross-section helps to save huge time and labor, and provide a more objective cotton sample maturity results. The previous FIAS overestimated 9% the maturity level of bale cotton because a lot of immature fibers could not be detected correctly. We also found that previous studies only used the mean of the cotton maturity (M_θ) to describe the bale cotton is not sufficient. Distribution shapes will vary even with the same mean value.

This thesis reports our efforts on developing a new FIAS system with the goal of a more precise cross-section detection. More statistic parameters, including mean (M_θ) , standard deviation (SD_θ), skewness (S_θ) and kurtosis (K_θ) are introduced in this study to provide a more comprehensive maturity understanding of cotton samples.

New hardware is set-up for the system, including a new modern trinocular microscope with a 10 times wider view area than the previous monocular microscope, and a digital single lens camera with a high image resolution.

Because the old FIAS failed to detect scratched, self-rolling, adhering, and contaminated cross-section, a novel coupled-contour model (*CCM*) of cotton cross-sections is proposed. Besides the cross-section and lumen contours, *CCM* also traces a cross-section inner contour which provides more information for a cross-sectional shape determination. Triangle-Area Representation (*TAR*) is introduced to check the shape of a cross-section. If the detected inner contour and outer contour have different *TAR*

descriptors, a further processing is required. By utilizing the inner contour information, individual cross-sections are separated from an adhering cross-section; the shapes of self-rolling or contaminated cross-sections can be corrected; and the lumens inside scratched are properly identified.

Compared the proposed algorithm detected results with manually cross-section tracing results of 7 of 104 selected cottons, a high correlation (R^2 =0.985) can be found, which demonstrates that the proposed algorithm is able to provide an almost same accurate cross-section detection result as human visualization analysis does. Locating contours, splitting inner contours, merging inner contours, refining outer contours, splitting adhered cross-sections, and refining contours are seven major steps of the algorithm. In evaluating the algorithm time efficiency, time consumptions of 7 cottons are acceptable, i.e. within the range 60 - 90 seconds. If more cross-sections are detected in a cotton or more cross-sections need further refinement, a longer processing time will be caused.

104 cottons with 15473 fiber cross-section images are examined under the new FIAS system. For each cotton, fiber contents (dead, immature, or mature) are calculated according to the average cross-sections maturity. However, of the 104 cotton, most of them can conclude as immature cotton because the immature fiber contents occupy the most portion of every sample, expect cotton 3089. The introducing of maturity distribution makes the 104 cottons more distinguishable. According to the skewness value, the fiber maturity is divided into 5 classes, i.e. very low, low, moderate, high, and very high from class I to class V, respectively. Of the 104 cottons, 20 of them are classified into very low - Class I; 39 cottons are low- Class II; Moderate- Class III has 30

cottons; 14 cottons are categorized into high- Class IV; and only one cotton go into very high - Class V.

A comparison analysis is performed between AFIS and new FIAS. The maturity distributions of AFIS and FIAS are noticeably different. AFIS and FIAS have good correlations only in mean θ. AFIS tends to generate more normal, less skewed and more concentrated maturity distributions. FIAS provides diversified maturity distributions ranging from highly right-skewed (positive) to highly-left skewed (negative). In general, AFIS gives higher immature fiber contents and lower dead or mature fiber contents than FIAS.

6.2 SUGGESTED FUTURE WORK

In order to verify the proposed algorithm robust, more cross-sectional images should be captured from different equipment with different lighting sources. The software is expected a friendlier interface and easier operation for a user.

Currently, there is still no conclusion between AFIS and FIAS that which method provides a more accurate result of the fiber maturity. It is suggested that more different cotton maturity measurement methods, i.e. a measurement of cotton fiber longitudinal geometry, testing the strength of finishing yarn or fabric made by each cotton, and etc., can be introduced to determine the fiber quality.

The Moment Test can be used to evaluate the normality of a distribution. Box-Cox transformation can introduce to correct the non-normal situation to a normal distribution. Then the new maturity standard may be more distinguishable among 104 cottons.

Bibliography

[1] B. Xu and B. Pourdeyhimi, "Evaluating maturity of cotton fibers using image analysis: difinition and algorithm," *Textile Research Journal,* vol. 64, no. 6, pp. 330-335, 1994.

[2] R. L. Barker and D. W. Lyons, "Determination of fiber cross-sectional circularity from measurements made in a longitudinal view," *Journal of Engineering for Industry,* vol. 101, no. 1, pp. 59-64, 1979.

[3] B. Xu, S. Wang and J. Su, "Fiber image analysis. Part III: A new segmentation algorithm for autonomous separation of fiber cross-sections," *Journal of the Textile Institute. Part 1, Fibre science and textile technology,* vol. 90, no. 3, pp. 288-297, 1999.

[4] B. D. Raskopf, "Micronaire tests for cotton and cotton quality relationships," 1966.

[5] J. M. Bradow, O. Hinojosa, L. H. Wartelle, G. Davidonis, G. F. Sassenrath-Cole and P. J. Bauer, "Applications of AFIS fineness and maturity module and x-ray fluorescence spectroscopy in fiber maturity evaluation," *Textile Research Journal,* vol. 66, no. 9, pp. 545-554, 1996.

[6] D. P. Thibodeaux and J. P. Evans, "Cotton fiber maturity by image analysis," *Textile Research Journal,* no. 56, pp. 130-139, 1986.

[7] D. P. Thibodeaux and J. B. Price, "Reference method for determination of the maturity of cotton fibers," *Melliand Textilberichte,* vol. 70, no. 4, pp. 243-246, 1988.

[8] B. Xu, B. Pourdeyhimi and J. Sobus, "Fiber cross-sectional shape analysis using image processing techniques," *Textile Research Journal,* vol. 63, no. 12, pp. 717-730, 1993.

[9] D. P. Thibodeaux and K. Rajasekaran, "Development of new reference standards for cotton fiber maturity," *Journal of Cotton Science,* vol. 3, no. 4, pp. 188-193, 1999.

[10] C. T. Inc., "Morphology characterization of cotton fibers," Clemex Image Analysis Report #135, 2001.

[11] B. Xu and Y. L. Ting, "Fiber-image Analysis Part I: Fiber-image Enhancement," *Journal of the Textile Institute,* vol. 87, no. 2, pp. 274-283, 1996.

[12] E. Hequet and B. Wyatt, "Relationship among image analysis on cotton fiber cross sections, AFIS measurements and yarn quality," *the Proceedings of the Beltwide Cotton Conference,* vol. 2, pp. 1294-1298, 2001.

[13] B. Xu and Y. Huang, "Image analysis for cotton fibers part II: cross-sectional measurements," *Textile Research Journal,* vol. 74, no. 5, pp. 409-416, 2004.

[14] E. F. Hequet, B. Wyatt, N. Abidi and D. P. Thibodeaus, "Creation of a set of reference material for cotton fiber maturity," *Textile Research Journal,* vol. 76, no. 7, pp. 576-586, 2006.

[15] L. Padmaraj, M. Krifa and B. Xu, "Evaluating immature fiber bias in fiber cross-section analysis," in *Proceedings Beltwide Cotton Conferences*, Atlanta, 2011.

[16] X. Guo, W. Ouyang and B. Xu, "Assessing cotton maturity using distributional parameters of fiber cross-section measurements," *Textile Research Journal,* vol. 84, no. 15, pp. 1666-1676, 2014.

[17] D. R. Paudel, E. F. Hequet and N. Abidi, "Evaluation of cotton fiber maturity measurements," *Industrial Crops and Products,* vol. 45, pp. 435-441, 2013.

[18] E. Lord, "Air flow through plugs of textile fibres: Part II. The micronaire test for cotton," *Journal of the Textile Institute Transactions,* vol. 47, no. 1, pp. 16-47, 1956.

[19] E. K. Boylston, D. P. Thibodeaux and J. P. Evans, "Applying microscopy to the development of a reference method for cotton fiber maturity," *Textile Research Journal,* vol. 63, no. 2, pp. 80-87, 1993.

[20] E. K. Boyiston, J. P. Evans and D. P. Thibodeaux, "A quick embedding method for light microscopy and image analysis of cotton fibers," *Biotechnic & histochemistry,* vol. 70, no. 1, pp. 24-27, 1995.

[21] F. T. Peirce and E. Lord, "The fineness and maturity of cotton," *Journal of the Textile Institute Transactions,* vol. 30, no. 12, pp. 173-210, 1939.

[22] Q. Wang and B. Xu, "A coupled-contour model for effective segmentation of cotton cross-sections in wide-field microscopic images," *Textile Research Journal,* p. 0040517516654113, 2016.

[23] X. Guo, W. Ouyang and B. Xu, "Shape recognition of profiled fibers using triangle-area representation," *Measurement Science and Technology,* vol. 24, no. 9, p. 095401, 2013.

[24] N. Alajlan, I. E. Rube, M. S. Kamel and G. Freeman, "Shape retrieval using triangle-area representation and dynamic space warping," *Pattern Recognition,* vol. 40, no. 7, pp. 1911-1920, 2007.

[25] T. Kosorl, K. Yawichai and Y. Kitjaidure, "Optimum shape representation based on Fisher's discriminant analysis," in *Electrical Engineering/Electronics, Computer, Telecommunications and Information Technology, 2008. ECTI-CON 2008. 5th International Conference*, 2008.

[26] B. Xu, L. Tang, P. Zeng and R. Wang, "Characterizing profiled fibers by multiscale shape representations," *Journal of Testing and Evaluation,* vol. 40, no. 3, pp. 435-439, 2012.